

We thank the reviewers for their thoughtful comments that have helped us clarify and improve the manuscript. We have reproduced the reviewer comments in black text. For ease of review, our responses are given in blue text, while the text added to the manuscript is given in *blue Italics*.

Referee 1 Comments

R1.1. This paper describes modeling the secondary organic aerosol (SOA) formation in Los Angeles as measured during the CalNex study in May/June 2010. The paper evaluates a variety of different models/parameterizations – WRF-CHEM, WRF-CMAQ, and a box model with several different mechanisms. None of the models are novel, but applying them to CalNex is new (EPA has been doing some evaluation of the CMAQ model, e.g. a paper is up on ACPD right now <http://www.atmos-chem-physdiscuss.net/15/157/2015/acpd-15-157-2015.html>). Given the comprehensive nature of the CalNex dataset it is valuable to use it to evaluate SOA models. The analysis is similar to previous work the authors have published for Mexico City.

The conclusions from the work appear to be largely consistent with those of previous studies. The old, traditional SOA models that only consider a relatively small number of volatile organic compounds cannot explain the measured SOA, even if one makes extreme corrections to yields for potential vapor wall losses to chamber walls. The paper shows that mass closure on the SOA can be achieved if one includes semivolatile and intermediate volatility precursors in a model. The paper evaluates several different schemes for doing this. The paper evaluates models against SOA mass, degree of oxygenation, and fossil/modern split. The parameterization with IVOC/SVOC all appear to work reasonably well (but not perfectly), but are not well constrained with data. The simple IVOC/SVOC schemes the authors consider appear to overpredict the amount of SOA at longer time scales (~ 3 days), presumably (as mentioned by the authors) because they do not include any fragmentation. There is reasonable agreement between fossil/modern carbon data and their apportionment. Finally, the authors show that a simple parameterization they developed in Mexico City for SOA formation appears to work in LA as well. These are basically the same set of conclusions as the Mexico City work, with the addition of fossil/modern carbon.

This is a well written paper. It is long and very comprehensive, but I found it not difficult to read and follow. It makes a contribution. Its weakness is that it does not break much new ground. There is value to show that they largely reach the same conclusions as they did with Mexico City. I would recommend the paper for publication after the authors address the following comments.

We thank the reviewer for his/her good summary of the paper and comments.

We note that it is not obvious that the results from LA were going to be similar to those from Mexico City, and many scientists had expressed skepticism that this would be the case. For example a prominent EPA scientist stated in a public comment on a past ACPD paper that “I haven’t paid enough attention to Mexico City modeling studies in the past because [...] I did not expect the findings from intensive field campaigns in Mexico City to be generally transferable when modeling other less-polluted regions of the world.” [P. Bhave, Atmos. Chem. Phys. Discuss., 10, C878–C884, 2010].

R1.2. “The work presented here quantitatively demonstrates that PAHs are relatively unimportant compared to other precursors such as methylbenzenes” This statement is too strong. The model only included a few PAH (naphthalenes, methylnaphthalene). It seems clear that these PAHs do not appear to be major precursors, but large amounts of unspciated IVOCs include a fair number of more alkylated or funcationalized PAHs. The authors claim that unspciated IVOC are mainly alkanes, but that has not really been established. If a reasonable fraction (10s of %) were PAHs then PAHs could play an important role.

We have substantially modified the relevant discussion and, for reference, have pasted the new text below.

“Figure 5B also shows a comparison for the naphthalenes. The tracer estimates are over an order-of-magnitude higher than the model predictions when using the SOA yields from the literature (which are ~20% for the conditions of our study) and the emission ratios determined from the regression analysis of nighttime measurements shown in Figure SI-3. The model is also

run using the empirically adjusted emission ratios that better match the observed concentrations of the naphthalenes. The model for this variation is still much lower than the tracer estimate. As an additional sensitivity study, we also run the model with the adjusted emissions and a yield of 150% that places all the oxidized mass in the $C^*=1 \mu\text{g m}^{-3}$ volatility bin. This last variation represents an upper limit estimate of SOA from naphthalenes, in which nearly all of the mass plus the added oxygen partitions to the particle phase, which is much higher than laboratory observations. The tracer estimate, however, is still about a factor of two higher than the model. It is known that the tracer estimate is an upper limit, because the tracer compound, phthalic acid, may not be a unique tracer, and it potentially could be emitted from primary sources (Kleindienst et al., 2012). However, there may be other alkylated or functionalized PAHs that are not explicitly accounted for in the box model, and some of them might produce the tracer.

The best estimate from the model with the adjusted emissions results in 0.7% of the predicted SOA being formed from the measured naphthalenes. Utilizing the upper limit of the model results for the PAHs, including that from the parameterization with a purposefully high yield, it is apparent that naphthalene, 1-methyl naphthalene, and 2-methyl naphthalene account for less than 4% of the SOA mass. While previous work has suggested that PAHs are important precursors for SOA in the Los Angeles Basin (Hersey et al., 2011) these earlier findings were qualitative and based on the observation of phthalic acid in samples. The work presented here, both the modeling results as well as the tracer results, quantitatively demonstrates that SOA from identified PAHs is relatively small but not negligible when compared to the total SOA concentration. An upper limit for the contribution of this group of precursors is $8(\pm 3)\%$ of the SOA. This percentage is calculated using the tracer method in which the SOA concentration from PAHs is higher than in the box model and a 30% uncertainty for the SV-OOA concentration. Lastly, we note that no suitable tracers for alkane oxidation have been identified yet, which prevents carrying out similar model/tracer comparisons with respect to the P-S/IVOCs, since these compounds are thought to be composed primarily, although not exclusively, of alkanes.”

R1.3. The authors should report the effective yields of the SI-SOA precursors. How do they compare of the recent work of Jathar (PNAS, 2014), which derived yields from chambers? How do they compare to the yields proposed by Zhao (EST, 2014) who performed this sort of model

with more extensive set IVOC data? How do they compare to smog chamber data for traditional precursors (alkanes, aromatics, etc.)?

The questions posed by the reviewer regarding the effective yields are very interesting. We have responded to them by adding the following paragraph to Section 3.1.1.

“In addition, the effective SOA yields predicted in the box model for P-S/IVOCs can be compared against those determined in previous modeling and smog chamber studies. The effective yield is a function of photochemical aging, and thus for the purpose of this comparison we focus on the effective box model yields for 12:00 – 15:00 when there was a moderate amount of photochemical aging (5 h at an average OH concentration of 1.5×10^6 molecules cm^{-3}) comparable to the degree of aging typically achieved in chambers. During this period the effective yields for P-S/IVOCs were 12%, 27%, and 36% for ROB+TSI, GRI+TSI, and PYE+TSI, respectively. Zhao et al. (2014) recently carried out a modeling study of SOA formed in Pasadena that was constrained with an extensive set of IVOC data and found an overall SOA yield for IVOCs of 29%, which falls within the range of effective yields for P-S/IVOCs that are predicted by the box model for the three different parameterizations. Jathar et al. (2014) also recently estimated from chamber studies an effective SOA yield of 10 – 40% for unspciated organic emissions from combustion sources, which is also consistent with the P-S/IVOC yields from our box model. For reference, the effective yields for the aromatic VOCs m-xylene, toluene, and benzene under high- NO_x conditions in chamber studies range from 4 – 28% depending on the precursor identity and chamber conditions (Ng et al., 2007). Similar chamber studies on 12-carbon alkanes determined effective yields ranging from 11% – 160%, where the highest yield corresponded to a cyclic alkane (Loza et al., 2014). In general, it appears that the effective yields resulting from the box model for the lower photochemical ages used here are similar to those determined from other chamber and modeling studies.”

R1.4. The paper uses the results to apportion SOA to different sources. Since the SVOC and IVOC concentrations are scaled with primary organic aerosol; this apportionment is presumably the same as the primary organic aerosol. The authors should clarify this point in the manuscript. I

suspect it is highly uncertain. For example, gasoline vehicles emit relatively little POA but likely contribute significant SOA (Jathar et al. 2014).

The reviewer is correct that the initial SVOC and IVOC concentrations are scaled from primary organic aerosols. However, the apportionment of SOA from P-S/IVOCs is not the same as that for primary organic aerosol, because the amount of SOA from each source is also a function of the photochemical age. For example, there are substantial cooking emissions in the evening, but these produce little SOA over the urban scale considered here, due to the short ambient photochemical ages at that time. In addition, the SOA apportionment takes account of SOA from VOCs, which are largely emitted by gasoline vehicles, and which are not scaled to POA.

Still, the reviewer is correct that in scaling the P-S/IVOCs to POA we have assumed that the P-S/IVOCs to POA ratio as well as the volatility distribution of P-S/IVOCs is the same for the different sources, which may not be accurate. To explain this uncertainty we have added the following paragraph to Section 3.1.4.

“The uncertainties in Figure 6 do not however account for certain assumptions that were made in order to perform the source apportionment. In particular, it was assumed that the P-S/IVOCs to POA ratio as well as the volatility distribution of P-S/IVOCs is the same for all sources, which is likely not the case. However, to our knowledge there is insufficient information in the literature to prescribe different volatility distributions for the different sources.”

R1.5. Zhao (EST, 2014) recently reported measurements of more IVOCs, including an estimate of the unspiciated IVOC. It appears that the naphthalene data came from the same dataset? How do the author’s estimates of unspiciated IVOC inferred from primary organic aerosol compare to the measured data of Zhao et al.? How do the predictions of the authors compare to Zhao et al.?

In response to this comment we have added a table to the supporting information (Table SI-3) that compares the estimated IVOCs from the model versus the measured data of Zhao et al. (2014). The table is also included below for the reviewer’s convenience. We have also added a paragraph to Section 3.1.1 that discusses the comparison (see quoted text below).

In addition, we have performed a sensitivity study in which all the IVOC emissions from cooking as well as diesel/gasoline have been reduced by one-half. This sensitivity study is summarized in a new paragraph in Section 3.1.5 (text is also quoted below).

“It is also possible to compare the predicted IVOC concentrations in the box model versus the concentrations measured by Zhao et al. (2014). The comparison is summarized in Table SI-3 of the supporting information. In total, the initial IVOC concentrations in the box model are two times higher compared to those determined from measurements ($16 \mu\text{g m}^{-3}$ versus $8(\pm 1) \mu\text{g m}^{-3}$). In addition, there is a larger difference for the $C^ = 10^3$ bin ($2.5 \mu\text{g m}^{-3}$ versus $0.2(\pm 0.1) \mu\text{g m}^{-3}$). At the same time, the model used by Zhao et al. to predict urban SOA is lower than the measurements by 50% on the urban scale, whereas as the box model used here does not exhibit such a low bias. Given these differences we have run two sensitivity studies to explore how the model predictions depend on the IVOC emissions that are discussed in the following sections. The first sensitivity study reduces the emission of P-S/IVOCs from cooking emissions to zero (Section 3.1.2), and the second sensitivity study reduces all IVOC emissions by one-half (Section 3.1.5). Both of these variations greatly improve the agreement between the modeled and measured IVOC concentrations.”*

“Table SI-3. Initial concentrations of primary IVOCs predicted by the box model (ROB parameterization) in comparison with data from Zhao et al. (2014) as a function of the saturation concentration (C^*) at 298 K. Note that the corresponding results for the GRI parameterization are very similar with the concentration being 8% higher due to differences in the ΔH_{vap} .

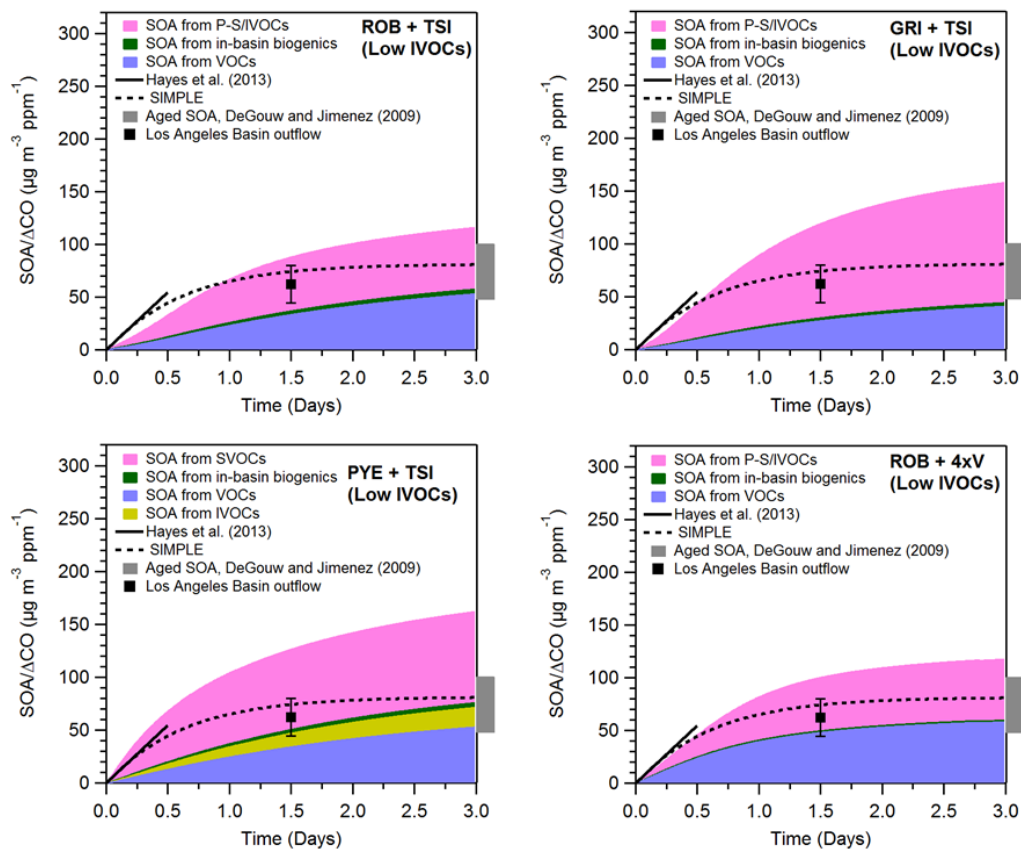
C^* ($\mu\text{g m}^{-3}$)	Estimated Primary IVOCs ($\mu\text{g m}^{-3}$)	Estimated Primary IVOCs without cooking emissions ($\mu\text{g m}^{-3}$)	Measured Primary IVOCs ($\mu\text{g m}^{-3}$)
10^3	2.47	1.70	0.21 (± 0.07)
10^4	3.30	2.27	1.39 (± 0.29)
10^5	4.12	2.84	2.64 (± 0.64)
10^6	6.59	4.54	3.82 (± 0.99)

From Section 3.1.5:

“A third explanation is the potential overestimation of IVOC emissions in the box model. As discussed in Section 3.1.1, the initial concentration of primary IVOCs in the model is a factor of 2 higher than the values determined from field measurements by Zhao et al (2014). To investigate this possibility, a sensitivity study was run in which the initial concentrations of primary IVOCs in the volatility bins $C^= 10^3, 10^4, 10^5, \text{ and } 10^6$ were decreased by one-half. The results of this sensitivity study are shown in Figure 8. In general, ROB+TSI, GRI+TSI, PYE+TSI, and ROB+4xV all show better agreement with measurements at long photochemical ages, although all four variants still overestimate the measurements. For shorter photochemical ages (in the urban scale) ROB+TSI under-predicts the SOA concentration, whereas GRI+TSI and ROB+4xV both predict SOA/ ΔCO ratios that are not significantly different from the measured values (Hayes et al., 2013), and lastly PYE+TSI overestimates the SOA concentration.*

Thus, IVOCs emissions that are too high in the box model may be responsible for some, but not all, of the overestimation of SOA concentrations at long photochemical ages.

For reference, we note that when the IVOC concentrations are halved the four variations all predict less SI-SOA for the Pasadena ground site (Figure SI-7), but the contribution of P-S/IVOCs to SOA formation remains important: 59 – 73% (ROB+TSI), 72 – 80% (GRI+TSI), 79 – 92% (PYE+TSI), 38 – 48% (ROB+4xV). Furthermore, all four variations still predict a fossil fraction of urban SOA consistent with the ^{14}C measurements at the Pasadena site: 66(\pm 9)%, 64(\pm 10)%, 61(\pm 12)%, 78(\pm 6)%, respectively. Note that in calculating these fossil fractions the IVOCs emissions from cooking and gasoline/diesel were reduced by the same amount (i.e. one-half).”



“Figure 8: SOA concentration predicted by the ROB+TSI, GRI+TSI, PYE+TSI, and ROB+4xV parameterizations for up to 3 days of photochemical aging at a reference $\cdot\text{OH}$ concentration of $1.5 \times 10^6 \text{ molec cm}^{-3}$. These predictions correspond to the sensitivity study in which the concentration of IVOCs in the volatility bins $C^* = 10^3 - 10^6$ were reduced by one-half. Also

shown in the three panels is the same result for the SIMPLE model using the optimized parameters (see Section 3.3 for further discussion). Note that the SOA concentrations have been normalized to the background subtracted CO concentration to account for changes in emission strengths, and the processed data are identified by the symbol SOA/ Δ CO. In addition, the SOA/ Δ CO data determined for the Pasadena site from the measurements of Hayes et al. (2013) are shown (black line) as well as similar airborne measurements downwind of Pasadena performed by Bahreini et al. (2012) aboard the NOAA P3 (black marker). The Bahreini et al. point corresponds to an average of all LA Basin outflow data between 1 – 2 days of photochemical aging. The OA/ Δ CO ratio reported by de Gouw and Jimenez (2009) is also indicated (gray box) to serve as an estimate of OOA/ Δ CO in highly aged air masses.”

R1.6. “Indeed, decreases in SOA concentration at high photochemical ages have been observed in flow-tube studies, although typically at photochemical ages much longer than 3 days (George and Abbatt, 2010).” More recent flow tube studies (Lambe et al. EST 2013; Tkacik et al. EST 2014) suggest that the fall off may occur at shorter photochemical ages (between 2 and 3 days).

The shorter photochemical ages in the Tkacik et al. study are not a real difference, but rather the result of that study using a higher OH concentration for the calculation of the ages. The decrease in the Tkacik et al. data occurs at 5 days, when one uses the same OH = 1.5×10^6 molec cm⁻³ used in this paper. Lambe et al. (ES&T 2013) does not include any such data. The reviewer may have meant to cite Lambe et al. (ES&T 2012), for which the decreases are observed between 4-8 days of equivalent exposure at OH = 1.5×10^6 molec cm⁻³.

In addition the apparent losses in recent flow tube studies where the SOA is formed in the reactor may be due to lack of SOA formation (e.g. due to oxidation of semivolatile species before they have time to condense, leading to fragmentation). The studies of George and Abbatt started with pre-existing OA and would not suffer from that potential problem, and thus we consider them more trustworthy for this point. Thus, we have not modified the text in response to this comment.

R1.7. SIMPLE parameterization is interesting. It is not clear how much fitting versus predicting is being done. This needs to be clarified in the manuscript. It appears that it has been retuned for

CalNex. If so then that is not as impressive – it is just a curve fit. If it is using previous parameters then that would be good. It would be interesting to better characterize the atmospheric conditions under which it may be applicable / influence SOA formation (VOC/NO_x, etc.). Presumably LA and Mexico City are pretty consistent.

We have modified the text to clarify the discussion of the SIMPLE parameterization (see below). We agree with reviewer that it would be interesting to better characterize the performance of SIMPLE under various atmospheric conditions and have noted this now in the text. We also note that we are proposing this parameterization for urban SOA sources, and not for, e.g., biogenic SOA. It is difficult to carry out the characterization described by the reviewer for our case study, however, due to the limited set of atmospheric conditions explored. For example, in Los Angeles high-NO_x conditions are generally observed. Thus, we recommend that future modeling studies also apply this parameterization to studies in other locations.

“We replaced the SOA parameterizations discussed above with the SIMPLE parameterization just described, and ran the box model for a large number of possible parameter value combinations (i.e. emission ratio of VOC/CO and ·OH rate constant). Figure 11A shows the difference between model and measurements over that parameter space. The diurnal cycle predicted by the SIMPLE parameterization with the optimum parameters for Pasadena is shown in Figure 11B. The SIMPLE model with the optimized parameters performs comparably to the more complex parameterizations used in this work. At the same time, the SIMPLE parameterization is unable to capture perfectly the location of the peak in time because it depends solely on CO and photochemical age. The CO concentration at the site peaks at 12:00 and photochemical age peaks at 13:00 (Figure 3A) while the measured SOA has a broad peak between 14:00 – 16:00. The fact that SOA does not peak at the same time as CO and photochemical age indicates the assumption in SIMPLE that VOC*/CO does not vary in time is probably not completely accurate. Still, the performance of the SIMPLE parameterization for urban SOA is sufficient for many applications and certainly far better than many models currently used.*

Interestingly, the optimal model parameters for Mexico City and Pasadena are very similar. In other words, when tuning the model separately for each city, the parameters obtained

are identical within the estimated uncertainties. This result suggests SIMPLE, with the parameters reported for Mexico City or Pasadena, can be applied to other polluted urban regions as well. In addition, the optimal parameters for Pasadena (and Mexico City) are consistent with the OA/ Δ CO ratios observed for highly aged air masses by Bahreini et al. (2012) from the NOAA P3 aircraft in the LA basin outflow, as well as for other urban areas as summarized by de Gouw and Jimenez (2009) and shown in Figure 7. However, it should be noted that a range of SIMPLE parameter combinations still remains in which the different combinations perform similarly in the model/measurement comparison, and this range is indicated by the dashed box in Figure 11A. While the SIMPLE model is promising, additional work should be carried out to verify the optimal SIMPLE model parameters including analysis of data for a broad range of ages, e.g., by utilizing results from ambient air processed by oxidation flow reactors (Ortega et al., 2013). Also, the accuracy of the SIMPLE model for predicting urban SOA under a variety of atmospheric conditions should be explored (e.g. VOC/ NO_x or relative amounts of gasoline versus diesel emissions.) Finally, we note that the SIMPLE model parameterizes urban SOA, and is not applicable to biogenic SOA.”

R1.8. The importance cooking emissions to SOA formation is interesting. I am not aware of data to support this. I believe that the 1.5 factor of Robinson et al. (Science 2007) is based on data for combustion sources. Is there evidence from source test data that it might also apply to cooking? What evidence is there for SOA from cooking?

This is an excellent question. In essence, there is evidence for SOA from cooking, but the number of studies and thus constraints available for developing cooking SOA parameterizations is currently very limited. In particular the Prévôt group at PSI (coauthors in this paper) has a paper in preparation detailing results from one extensive study where significant SOA formation was clearly observed, and that has been presented at the AAAR Annual Meeting and other conferences.

We hope that our study will highlight the potential importance of cooking SOA and motivate further work on this topic. We have added the following paragraph to the end of Section 3.1.4 in

order to better explain the potential importance as well as the uncertainty regarding cooking SOA.

“Lastly, the percentage of SOA attributed to cooking emission in this work also requires discussion. Compared to gasoline or diesel vehicles there is relatively little data on the SOA forming potential of cooking emissions, but nevertheless there is both direct and indirect data supporting the SOA forming potential of cooking emissions. First, it is clear from numerous source apportionment studies that cooking emissions are a source of organic matter in the atmosphere (e.g. Robinson et al., 2006; Mohr et al., 2011; Hayes et al., 2013). Second, molecular speciation of cooking emissions has demonstrated that cooking activities emit a variety of volatile and semi-volatile compounds that are known SOA precursors (Schauer et al., 1999, 2002). Third, chamber studies have demonstrated SOA formation from cooking emissions. The latter results have been presented at several major conferences, but not yet been published in the peer-reviewed literature (El Haddad et al., 2012). Thus, it is reasonable to conclude that SOA models should include the SOA resulting from chemical processing of cooking emissions, but there is a lack of chamber yields that could be used to develop specific SOA parameterizations. We have therefore assumed that SOA from cooking emission can be described using the same parameterizations as used for SOA from vehicular P-S/IVOCs. We also perform a sensitivity study where we assume that cooking emissions do not produce any SOA. Ultimately, the percentage of SOA from cooking emissions reported here should be considered a first-order estimate that should be updated when additional data regarding SOA from cooking emissions becomes available.”

References.

Jathar, S. H.; Gordon, T. D.; Hennigan, C. J.; Pye, H. O. T.; Pouliot, G.; Adams, P. J.; Donahue, N. M.; Robinson, A. L., Unspeciated organic emissions from combustion sources and their influence on the secondary organic aerosol budget in the United States. Proceedings of the National Academy of Sciences 2014, 111, (29), 10473-10478.

Tkacik, D. S.; Lambe, A. T.; Jathar, S.; Li, X.; Presto, A. A.; Zhao, Y.; Blake, D.; Meinardi, S.; Jayne, J. T.; Croteau, P. L.; Robinson, A. L., Secondary Organic Aerosol Formation from in-Use

Motor Vehicle Emissions Using a Potential Aerosol Mass Reactor. *Environ. Sci. Technol.* 2014, 48, (19), 11235-11242.

Lambe, A. T.; Cappa, C. D.; Massoli, P.; Onasch, T. B.; Forestieri, S. D.; Martin, A. T.; Cummings, M. J.; Croasdale, D. R.; Brune, W. H.; Worsnop, D. R.; Davidovits, P., Relationship between Oxidation Level and Optical Properties of Secondary Organic Aerosol. *Environ. Sci. Technol.* 2013, 47, (12), 6349-6357.

Lambe, A. T.; Onasch, T. B.; Croasdale, D. R.; Wright, J. P.; Martin, A. T.; Franklin, J. P.; Massoli, P.; Kroll, J. H.; Canagaratna, M. R.; Brune, W. H.; Worsnop, D. R.; Davidovits, P., Transitions from Functionalization to Fragmentation Reactions of Laboratory Secondary Organic Aerosol (SOA) Generated from the OH Oxidation of Alkane Precursors. *Environ. Sci. Technol.* 2012, 46, (10), 5430-5437.

Zhao, Y.; Hennigan, C. J.; May, A. A.; Tkacik, D. S.; de Gouw, J. A.; Gilman, J. B.; Kuster, W. C.; Borbon, A.; Robinson, A. L., Intermediate-Volatility Organic Compounds: A Large Source of Secondary Organic Aerosol. *Environ. Sci. Technol.* 2014, 48, (23), 13743-13750.

We thank the reviewers for their thoughtful comments that have helped us clarify and improve the manuscript. We have reproduced the reviewer comments in black text. For ease of review, our responses are given in blue text, while the text added to the manuscript is given in *blue Italics*.

Referee 2 Comments

R2.1. Hayes et al. present results from box model simulations of in-basin SOA formation focusing on Pasadena, CA and measurements made during the CalNex 2010 study. Their box model is explicitly constrained by observations of ambient traditional VOC concentrations. They also include emissions of intermediate and semi-volatile organic compounds (I/SVOCs) that are not included in standard emissions inventories. They link their I/SVOC emissions to POA emissions and assume that all POA sources have identical volatility distributions. They also consider a first order estimate of the influence of chamber biases on SOA yields by multiplying their yields of semi-volatile VOC product species by 4. They have considered a number of different schemes for treating the oxidation of S/IVOCs and even of VOCs. They find that the various combinations all exhibit a diurnal profile shape consistent with the observations, but that certain model formulations perform better than others when the model results are compared with observations of the semi-volatile oxygenated organic aerosol (SV-OOA) factor determined from PMF analysis of the ambient organic aerosol time-series. They conclude that, overall, there is a need for some contribution of I/SVOCs to allow for simulation of SOA levels that are consistent with the average SV-OOA diurnal profile. They find that biogenics from within LA (“in-basin”) contribute negligibly to the total in-basin SOA, although biogenic-SOA may contribute to the background OA burden. They find when they extrapolate their simulations based on these literature parameterizations to longer times that they overestimate the amount of SOA that should be formed.

Overall, the authors do a good job explaining what they have done, describing the results, and comparing between the different literature model formulations. I believe that this work should be publishable after they address the comments below.

We thank the referee for their thoughtful review and have provided point-by-point responses to their comments below.

R2.2. The authors apply a number of different model formulations, taken from the literature, for the simulation of SOA concentration diurnal profiles within a constrained box model. Each of these model formulations/parameterizations has particular limitations that ultimately lead to differences in the box model results. Some aspects of the model formulations are more constrained than others. For example, the VBS yields for the traditional VOCs are constrained from comparisons with chamber observations whereas the literature ageing scheme(s) applied have generally weak, or even no, constraints. The O/C parameterization for S/IVOCs are similarly underconstrained, while the O/C estimates for SOA from VOCs are guided by observations from laboratory studies. The S/IVOC emission scheme is linked to literature measurements of POA volatility, although connecting these observational constraints on the volatility distribution to actual emissions is challenged by a lack of knowledge regarding the conditions under which the emission inventory was determined. I therefore suggest that it would be useful if the authors were to note a bit more explicitly what aspects of the literature parameterizations are more/less constrained by previous observations. They already do a good job of describing the model formulations, but some minor addition regarding the nature of these formulations might facilitate greater understanding by the reader. I also suggest that, given the inherent uncertainties in the parameterizations, that the authors limit the scope of any conclusions regarding whether one particular parameterization is particularly better than another.

We generally agree with the descriptions of the reviewer in this comment. Some of the parameterizations are based on a larger amount of data than others, and some have only weak constraints. We have included all the constraints that we were aware of, but in some cases assumptions needed to be made due to the limitations of the available information. In all cases we have made what we thought was the most reasonable assumption, stated clearly what was done, and in multiple cases we have presented several model alternatives to illustrate the sensitivity of the results to different assumptions.

We have modified the abstract and the conclusions to better clarify these points. We have removed the sentence that stated that the GRI parameterization did better in reproducing the observations. In particular, the following text has been added to the abstract:

“The results from the 3 parameterizations show large differences (e.g. a factor of 3 in SOA mass) and are not well constrained, underscoring the current uncertainties in this area.”

and

“The relative contribution of each source is uncertain by almost a factor of 2 depending on the parameterization used.”

R2.3. Some additional clarification regarding the specification of the BVOC emissions would be useful.

We have added a paragraph to the manuscript to clarify the specification of the biogenic VOC emissions. As an example, we have also included in Figure SI-2 a comparison of the diurnal cycle predicted and measured for isoprene.

“The biogenic VOCs are not expected to be emitted proportionally with CO, and therefore the approach described in the previous paragraph cannot be used to specify the biogenic VOC emissions. Rather, the emissions of biogenic VOCs were adjusted empirically to match the observed concentrations of isoprene and terpenes, after accounting for anthropogenic isoprene using $\Delta(\text{isoprene})/\Delta\text{CO}$ (Borbon et al., 2013). Only ~4% of the daily average isoprene is from anthropogenic sources. In addition, the diurnal profile of emissions was assumed to be proportional to temperature.

The model consistency with the VOC measurements, including for biogenic VOCs, is evaluated by comparing the measured and modeled diurnal cycles. Some of the cycles compared are given in Figure SI-2 as an example. It is observed that the model is generally consistent with the biogenic VOC measurements.”

R2.4. P32340: The authors should provide some brief discussion regarding their use of a constant [OH] in the simulations.

We have added substantially more discussion regarding the use of constant [OH] in the simulations. Please see the updated text below, which is from Section 2.3.

“The second consideration is that the purpose of using the ratio of VOC concentrations is to determine the ·OH exposure for the air mass at the Pasadena site. (·OH exposure is the concentration integrated over time for an air parcel.) While the ·OH exposure for the site is therefore well-constrained, the actual ·OH concentration in the modeled air parcel as a function of time is not as well-constrained. Thus, the photochemical ages used here (Figure 3) are calculated using an average ·OH concentration of 1.5×10^6 molec cm^{-3} , as described in our previous work (Hayes et al., 2013), and the model is run with the same concentration. Insofar as the model produces the same ·OH exposure as determined from measurements, which is always the case in this modeling study, the actual concentration of ·OH used in the model is not expected to substantially influence the results. In other words, while the concentration ·OH in the model is assumed to be 1.5×10^6 molec cm^{-3} , the integral of the ·OH concentration over time is constrained by the observed VOCs ratios. As expected, in the middle of the day the photochemical age will be longer than the transport age, and the opposite will be true during periods with low ambient ·OH.”

R2.5. Section 2.6: Some clarification regarding the correction for “higher OA concentrations upwind of Pasadena” would be useful.

We have added a more in-depth introduction to this section in order to clarify this correction (see below). Perhaps, a useful way to understand this correction is the following: the initial concentration of precursors are calculated using the emission ratios to CO, which are multiplied by the measured excess CO (above the background level) to determine the initial precursor concentrations. Given that CO and precursors should undergo the same amount of vertical and horizontal dilution during transport, this approach implicitly dilutes the precursors by the appropriate factor before oxidation occurs. In reality, the species in the air parcel are oxidized

and diluted at the same time. This difference then means that the partitioning calculated in the model upwind of Pasadena will not be perfectly accurate. (However, the partitioning calculated at Pasadena is accurate.) We have applied a correction for this effect, although this correction is actually small due to the fact that the aerosol mass is distributed in volatility space over many orders of magnitude, whereas the OA concentration generally varies over a much smaller range (2 - 20 $\mu\text{g m}^{-3}$ for Pasadena).

“2.6. Correction for changes in partitioning due to emissions into a shallower boundary layer upwind of Pasadena

To account for changes in partitioning due to lower planetary boundary layer (PBL) heights, and thus, increased OA concentrations upwind of Pasadena, the concentrations of POA, V-SOA, and SI-SOA are increased upwind of Pasadena beyond the amount already simulated in the model. This correction is necessary because using CO as a conservative tracer of emissions does not account for how the shallow boundary layer over Los Angeles in the morning influences partitioning between the gas and particle phases. Specifically, during the afternoon Pasadena is a receptor site for pollution from downtown Los Angeles that was generally emitted into a shallower boundary layer during the morning. The reduced vertical dilution will lead to higher concentrations of POA as well as any urban SOA formed, which in turn leads to higher partitioning to the particle phase and less gas phase oxidation of primary and secondary S/IVOCs.”

R2.6. Questions and concerns regarding results and discussion:

I suggest that the introduction of the model variant that considers the influence of vapor wall losses be moved to methods.

In accordance with the reviewer’s comment we have moved this subsection to the methods section.

R2.7. P32347/L10: The authors conclude here that their simulation results point to the “importance” of S/IVOCs. “Importance” is such a cagey word. I suggest that the authors be more

precise, stating that their results suggest that S/IVOCs contribute anywhere from X-Y% of the total SV-SOA.

We agree with the review that giving a percentage would be more precise, and so we have calculated the percentage of SOA formed from P-S/IVOCs in each model and added text describing the results to the manuscript (see quoted text below).

“Specifically, the contribution to total SOA from P-S/IVOCs in the box model is 65-75% (ROB+TSI), 80-87% (GRI+TSI), 80-92% (PYE+TSI), and 44-51% (ROB+4xV). The range indicates the variation in the contribution with the time-of-day. Thus, only in the ROB+4xV model variation is the estimated contribution to SOA from VOCs generally larger than or equal to that from the P-S/IVOCs. We note however these percentages include only the urban SOA and not the background OA, which is likely also SOA.”

R2.8. Although the authors do clearly distinguish between SV-OOA and LV-OOA, in general, it could be useful if they take opportunities to remind readers more often that the SOA being investigated here excludes background OA, a fraction of which is likely SOA.

We have added several reminders of this point to the text. In particular, these reminders have been added to the 1st paragraph of Section 3.1.1., the first paragraph of Section 3.1.2., and the figure caption of Figure 6.

R2.9. Fossil vs. Modern: 1. The fossil/modern carbon analysis was determined for samples collected over only 7 days, a small subset of the overall campaign. The authors should note whether this week was generally representative of the overall campaign. 2. The authors might point out more strongly that the fossil/modern split determined here is linked to the assumptions regarding the assumed I/SVOC volatility distributions and emissions of these same compounds between sources.

In accordance with the reviewer’s first comment we have added the following text to Section 2.4.

“In particular, the dates that the filters were collected were 30 May as well as 3, 4, 5, 6, 13, and 14 June 2010. Thus, these filters are more representative of the second half of the campaign that was more strongly influenced by pollution from the basin, compared to the first half of the campaign where regional advection played a more important role (Ryerson et al., 2013). Given the cost of the ^{14}C analyses, these days were chosen on the basis of the larger urban influence determined from the real-time measurements, and are therefore better suited to constrain urban sources (the subject of this paper) than if the analyses had been performed on filters from randomly-chosen days. However, it is noted that the relative concentrations of the different components of the OA were similar when averaging the second half of the campaign or the entire campaign: 14% vs. 12% for HOA, 5% vs. 5% for LOA, 12% vs. 17% for COA, 28% vs. 34% for LV-OOA, 40% vs. 34% for SV-OOA. Thus, it appears reasonable to assume that the relative results from the ^{14}C analysis are representative of the entire campaign. ”

With respect to the second comment, we have added the following discussion to Section 3.1.2.

“It should be noted that the fossil/modern split from the box model that is described above depends on the initial P-S/IVOCs concentrations and volatility distribution assumed in the model. These parameters are not well constrained for cooking emissions, as discussed in further detail in Section 3.1.4 below. In addition, as discussed in the previous section (3.1.1) the concentration of primary IVOCs in the box model is higher than that measured. Thus, as an extreme sensitivity study, the model variations were also run under the assumption that cooking sources did not emit any P-S/IVOCs or, in the case of the PYE+TSI variation, any SVOCs (Figure SI-5). In this sensitivity study there is improved model/measurement agreement for primary IVOCs as shown in Table SI-3.”

R2.10. SOA Apportionment: P32354/L14: I find the point associated with the mention of these PMF results from filters to be somewhat unclear. Are the authors simply saying that someone else said that diesel might contribute something?

Yes, that is correct. We have modified the text to make this point clearer (see quoted text below.)

“In addition, the existence of a diesel contribution in the model is consistent with PMF analysis of FTIR spectra of OA filter samples collected in Pasadena, in which, one SOA component exhibited relative peak intensities in the C-H stretching region that suggest some contribution from diesel emissions (Guzman-Morales et al., 2014), although the percentage of SOA from diesel could not be determined in this previous work.”

R2.11. Evolution for 3 days: P32356/L12: I can see the concern raised regarding potential overestimates of OA downwind from urban regions in models. However, I think it is equally important to note that this is intimately tied to the model formulation that is used. Many models use very simple parameterizations that will not overpredict (necessarily), potentially even underpredicting (as shown with the WRF-CMAQ model). I think that the model dependency of this conclusion needs to be emphasized to a greater extent.

We have updated the text in this section (3.1.5) to more clearly state that this finding only applies to the parameterizations discussed in this section. The revised text reads:

“We also note that all of the parameterizations used in this section produce SOA/ Δ CO ratios substantially larger (by factors of 2 or more) than those observed globally for aged air masses (i.e. photochemical ages greater than one day at an average OH concentration of 1.5×10^6 molec cm^{-3}).”

R2.12. WRF-CMAQ box modeling: I think that the comparison here can go even further than what is already noted by the authors. The non-ageing VBS treatment of VOCs in the primary box model is essentially equivalent to the 2-product model in CMAQ. The only difference is really that there are four products instead of two. Yet in the primary box model if only the VOCs are considered the underprediction is not a factor of 25, as is seen when using CMAQ in box model form. It is more like a factor of 5 or 6. While still substantial, I think that this also indicates that there is a fundamental difference in the basic model parameters used in the CMAQ 2 product formulation vs. the VBS 4-product formulation. In other words, toluene in CMAQ does not equal toluene in VBS. The authors are encouraged to emphasize this upon revision. They may wish to

refer to (Barsanti et al., 2013) who discuss issues associated with refitting data to determine 2 product parameters.

The statement by the reviewer about the two parameterizations being “essentially equivalent” is incorrect. The two parameterizations of V-SOA are conceptually equivalent but produce substantially different results. As stated in P32357, L17-24, for this comparison we use the older V-SOA yields from Koo et al. (2003), which are significantly lower than those of the Tsimpidi et al. (2010) parameterization used in the rest of the paper. The latter parameterization was updated using more recent chamber results such as those of Ng et al. (2007). We use the Koo et al. (2003) parameterization when comparing the results of the box model to WRF-CMAQ because the parameterization in CMAQ is of the same vintage, and thus we can show that both models produce very similar results when using similar parameterizations. We have added the following text at the end of P32357 L24 to clarify this point:

“Note that the Koo et al. (2003) parameterization produces substantially lower V-SOA yields than the Tsimpidi et al. (2010) parameterization used in the rest of this work. The latter parameterization was updated using more recent chamber results (with higher yields) such as those of Ng et al. (2007). The use of the older Koo et al. (2003) parameterization for this specific comparison was motivated by the fact that the parameterization for urban SOA in the version of CMAQ used here is based on the same older data, and does not contain the higher updated yields in, for example, Tsimpidi et al. (2010).”

R2.13. Oxygen content comparison: The literature oxygenation (i.e. O/C) parameterizations used for S/IVOCs are particularly underconstrained. I suggest that the authors take care to note that, given these inherent uncertainties in the O/C model formulation, the results here should not necessarily be taken as an indication that one model performs better than another.

We certainly agree with the reviewer, and have added the following paragraph in Section 3.2 of the manuscript in order to highlight this important point.

“Lastly, we note that there are large uncertainties in the parameters used to predict O:C such as the distribution of O:C values as a function of volatility for V-SOA or the amount of oxygen mass added to the SI-SOA for each oxidation reaction. It is therefore not very meaningful to conclude from this study that one parameterization performs better than another. Rather, it is apparent that when using several different previously published SOA parameterizations (i.e. ROB+TSI, GRI+TSI, and TSI alone) it is possible to reproduce the observed O:C at the Pasadena ground site.”

R2.14. The updated SOA budget: I suggest that the authors focus this discussion on the anthropogenic SOA budget, with less consideration given to the BVOC SOA budget, given that the (non-cooking related) urban SOA here is predominately anthropogenic in origin.

We agree with the reviewer that the BVOC SOA budget is highly uncertain and unrelated to the new constraints derived in this paper, and we have thus removed all references to this topic from the text.

R2.15. Conclusions: Given the differences between the different parameterizations regarding the relative contributions from S/IVOCs versus VOCs towards the urban SOA, I suggest that the authors further emphasize that the relative concentrations remain quite uncertain.

We agree with the reviewer and had already included a statement to this effect in the conclusions. However, we have added an additional sentence to the conclusions to emphasize the uncertainty in the relative contributions from each category of precursor. The updated text from the conclusions is quoted below.

“The relative importance of VOCs and P-S/IVOCs as contributors to urban SOA over different time and length scales remains unclear. Depending on the parameterization used in the box model, the amount of urban SOA from VOCs can range between 15 – 53% of the total predicted SOA for the Pasadena ground site. This range is 16 - 58% in a sensitivity study in which the IVOC emissions are reduced by one-half.”

R2.16. Figures: Figure 1 is fantastic and is very helpful to the reader to understand how the model formulations work.

We are very happy to hear that the referee found Figure 1 to be helpful.

References.

Barsanti, K. C.; Carlton, A. G.; Chung, S. H. Analyzing experimental data and model parameters: implications for predictions of SOA using chemical transport models. *Atmos. Chem. Phys.*, 13, 12073-12088, 2013.

Koo, B. Y.; Ansari, A. S.; Pandis, S. N. Integrated approaches to modeling the organic and inorganic atmospheric aerosol components. *Atmos. Environ.*, 37, 4757-4768, 2003.

Ng, N. L.; Kroll, J. H.; Chan, A. W. H.; Chhabra, P. S.; Flagan, R. C.; Seinfeld, J. H. Secondary organic aerosol formation from m-xylene, toluene, and benzene. *Atmos. Chem. Phys.*, 7, 3909–3922, 2007.

Tsimpidi, A. P.; Karydis, V. A.; Zavala, M.; Lei, W.; Molina, L.; Ulbrich, I.M.; Jimenez, J. L.; Pandis, S. N. Evaluation of the volatility basis-set approach for the simulation of organic aerosol formation in the Mexico City metropolitan area. *Atmos. Chem. Phys.*, 10, 525-546, 2010.

Modeling the formation and aging of secondary organic aerosols in Los Angeles during CalNex 2010

Patrick L. Hayes^{1,2,3}, Annmarie G. Carlton⁴, Kirk R. Baker⁵, Ravan Ahmadov^{1,6}, Rebecca A. Washenfelder^{1,6}, Sergio Alvarez⁷, Bernhard Rappenglück⁷, Jessica B. Gilman^{1,6}, William C. Kuster⁶, Joost A. de Gouw^{1,6}, Peter Zotter⁸, Andre S. H. Prévôt⁸, Sönke Szidat⁹, Tadeusz E. Kleindienst⁵, John H. Offenberg⁵, [Prettiny K. Ma³](#), Jose L. Jimenez^{1,2}

(1) Cooperative Institute for Research in Environmental Sciences (CIRES), University of Colorado, Boulder, CO, USA.

(2) Department of Chemistry and Biochemistry, University of Colorado, Boulder, CO, USA.

(3) Université de Montréal, Department of Chemistry, Montreal, QC, CANADA

(4) Department of Environmental Sciences, Rutgers University, New Brunswick, NJ, USA.

(5) US Environmental Protection Agency, Research Triangle Park, NC, USA.

(6) Earth System Research Laboratory, National Oceanic and Atmospheric Administration (NOAA), Boulder, CO, USA.

(7) Department of Earth and Atmospheric Sciences, University of Houston, TX, USA.

(8) Laboratory of Atmospheric Chemistry, Paul Scherrer Institute, Villigen, Switzerland.

(9) Department of Chemistry and Biochemistry & Oeschger Centre for Climate Change Research, University of Bern, Switzerland.

Correspondence to:

P. L. Hayes (patrick.hayes@umontreal.ca) and J. L. Jimenez (jose.jimenez@colorado.edu)

24 Abstract

25 Four different literature parameterizations for the formation and evolution of urban
26 secondary organic aerosol (SOA) frequently used in 3D models are evaluated using a 0-D box
27 model representing the Los Angeles Metropolitan Region during the CalNex 2010 field
28 campaign. We constrain the model predictions with measurements from several platforms and
29 compare predictions with particle and gas-phase observations from the CalNex Pasadena ground
30 site. That site provides a unique opportunity to study aerosol formation close to anthropogenic
31 emission sources with limited recirculation. The model SOA formed only from the oxidation of
32 VOCs (V-SOA) is insufficient to explain the observed SOA concentrations, even when using
33 SOA parameterizations with multi-generation oxidation that produce much higher yields than
34 have been observed in chamber experiments, or when increasing yields to their upper limit
35 estimates accounting for recently reported losses of vapors to chamber walls. The Community
36 Multiscale Air Quality (WRF-CMAQ) model (version 5.0.1) provides excellent predictions of
37 secondary inorganic particle species but underestimates the observed SOA mass by a factor of 25
38 when an older VOC-only parameterization is used, which is consistent with many previous
39 model-measurement comparisons for pre-2007 anthropogenic SOA modules in urban areas.

40 Including SOA from primary semi-volatile and intermediate volatility organic
41 compounds (P-S/IVOCs) following the parameterizations of Robinson et al. (2007), Grieshop et
42 al. (2009), or Pye and Seinfeld (2010) improves model/measurement agreement for mass
43 concentration. The results from the 3 parameterizations show large differences (e.g. a factor of 3
44 in SOA mass) and are not well constrained, underscoring the current uncertainties in this area.
45 ~~When comparing the three parameterizations, the Grieshop et al. parameterization more~~
46 ~~accurately reproduces both the SOA mass concentration and oxygen-to-carbon ratio inside the~~
47 ~~urban area.~~ Our results strongly suggest that other precursors besides VOCs, such as P-S/IVOCs,
48 are needed to explain the observed SOA concentrations in Pasadena. All the recent
49 parameterizations over-predict urban SOA formation at long photochemical ages (≈ 3 days)
50 compared to observations from multiple sites, which can lead to problems in regional and
51 especially global modeling. However, reducing IVOC emissions by one-half in the model to
52 better match recent IVOC measurements improves SOA predictions at these long photochemical
53 ages.

54 Among the explicitly modeled VOCs, the precursor compounds that contribute the
55 | greatest SOA mass are methylbenzenes. [Measured Polycyclic aromatic hydrocarbons](#)
56 | [\(naphthalenes\) contribute 0.7% of the modeled SOA mass.](#) The amounts of SOA mass from
57 | diesel vehicles, gasoline vehicles, and cooking emissions are estimated to be 16 – 27%, 35 –
58 | 61%, and 19 – 35%, respectively, depending on the parameterization used, which is consistent
59 | with the observed fossil fraction of urban SOA, 71(±3)%. [The relative contribution of each](#)
60 | [source is uncertain by almost a factor of 2 depending on the parameterization used.](#) In-basin
61 | biogenic VOCs are predicted to contribute only a few percent to SOA. A regional SOA
62 | background of approximately 2.1 $\mu\text{g m}^{-3}$ is also present due to the long distance transport of
63 | highly aged OA, [likely with a substantial contribution from regional biogenic SOA.](#) The
64 | percentage of SOA from diesel vehicle emissions is the same, within the estimated uncertainty,
65 | as reported in previous work that analyzed the weekly cycles in OA concentrations (Bahreini et
66 | al., 2012; Hayes et al., 2013). However, the modeling work presented here suggests a strong
67 | anthropogenic source of modern carbon in SOA, due to cooking emissions, which was not
68 | accounted for in those previous studies, [and which is higher on weekends.](#)

69 Lastly, this work adapts a simple two-parameter model to predict SOA concentration and
70 | O/C from urban emissions. This model successfully predicts SOA concentration, and the optimal
71 | parameter combination is very similar to that found for Mexico City. This approach provides a
72 | computationally inexpensive method for predicting urban SOA in global and climate models. We
73 | estimate pollution SOA to account for 26 Tg yr^{-1} of SOA globally, or 17% of global SOA, 1/3 of
74 | which is likely to be non-fossil.

75 **1. Introduction**

76 Submicron aerosols impact regional to global climate (IPCC, 2013), visibility (Watson,
77 2002), and human health (Dockery and Pope, 1994). Quantification of the environmental and
78 health impacts of atmospheric aerosols is difficult however, because of our incomplete
79 understanding of aerosol physical and chemical properties. Atmospheric aerosols are typically a
80 mixture of organic and inorganic matter, and the organic fraction is normally composed of
81 hundreds or even thousands of compounds. Due to this complexity, accurate prediction of OA
82 concentrations, as well as chemical properties is challenging (McKeen et al., 2007; Heald et al.,
83 2011; Spracklen et al., 2011). This problem is especially important given that OA represents
84 roughly half of the total tropospheric submicron aerosol mass in many environments including
85 polluted urban regions (Murphy et al., 2006; Jimenez et al., 2009).

86 Given its complexity, OA is often categorized based on sources. Primary organic aerosols
87 (POA) are emitted directly into the atmosphere from sources such as motor vehicles, food
88 cooking, and wildfires. SOA is formed in the atmosphere by photooxidation and/or
89 heterogeneous or cloud processing of gas-phase precursors. The gas-phase precursors for SOA
90 potentially have many sources including vehicle emissions, the biosphere, biomass burning, and
91 food cooking (e.g. Schauer et al., 1999; Hallquist et al., 2009; Hodzic et al., 2010b; Bahreini et
92 al., 2012). A large portion of the submicron OA throughout the world can be classified as SOA
93 (Zhang et al., 2007; Jimenez et al., 2009). Even in urban areas such as the Los Angeles
94 Metropolitan Area, SOA is often found to be larger than POA, especially in the summer
95 (Docherty et al., 2008; Hersey et al., 2011; Hayes et al., 2013).

96 Traditional models for SOA formation use a semi-empirical approach wherein SOA
97 formation is described in two steps: the gas-phase oxidation of VOC precursors resulting in the
98 formation of semi-volatile organic compounds (SVOCs), followed by partitioning of the SVOCs
99 to the particle phase. The parameters for these models (yields, saturation concentrations, etc.) are
100 typically derived from smog chamber experiments on individual VOCs (Hallquist et al., 2009).
101 Since about 2005, it has been shown in multiple publications from several field studies that
102 traditional models under-predict observed SOA in urban areas by a large amount with a
103 difference of up to a factor of 19. (Volkamer et al., 2006; de Gouw and Jimenez, 2009; Dzepina
104 et al., 2009; Hodzic et al., 2010a). A similarly large underestimate is typically not observed in

105 areas dominated by biogenic SOA (Tunved et al., 2006; Chen et al., 2009; Hodzic et al., 2009;
106 Slowik et al., 2010). In response, new precursors and pathways for SOA formation have been
107 identified from measurements and incorporated into SOA models. The new formation pathways
108 include SOA formation from primary semivolatile and intermediate volatility organic
109 compounds (P-S/IVOCs) (Robinson et al., 2007), aqueous phase production in clouds (e.g. Lim
110 et al., 2005) and aerosols (Ervens and Volkamer, 2010; Knote et al., 2014b), as well as the
111 oxidation of VOCs such as isoprene, benzene, and acetylene that were previously thought to
112 produce little or no SOA (Martin-Reviejo and Wirtz, 2005; Kroll et al., 2006; Volkamer et al.,
113 2009).

114 The introduction of the volatility basis set (VBS) approach represents a conceptual
115 advance for modeling OA (Donahue et al., 2006). This approach distributes organic species into
116 logarithmically spaced volatility bins, which are used to calculate absorptive partitioning
117 between the gas and particle-phases. Mass is transferred between the bins as photochemical
118 oxidation proceeds and environmental parameters (i.e. temperature, dilution) change. The VBS
119 approach has been applied to SOA from biogenic and anthropogenic VOCs as well as to P-
120 S/IVOCs and the SOA formed from them (Robinson et al., 2007; Tsimpidi et al., 2010).

121 Although these updates have led to substantial reductions in the gaps between observed
122 and predicted OA concentrations, major inconsistencies and uncertainties remain, and it is not
123 clear that improved agreement is achieved for the right reasons. For instance, both Dzepina et al.
124 (2011) and Hodzic et al. (2010a) reported that the Robinson et al. (2007) parameterization for the
125 production of SOA from P-S/IVOCs contributed substantially to successful predictions of SOA
126 concentration in a box and a regional model for the Mexico City region, but the predicted O/C
127 values were approximately a factor of 2 too low. A different parameterization of SOA from P-
128 S/IVOCs published by Grieshop et al. (2009) led to overpredicted total SOA concentration, but
129 successfully reproduced the measured O/C values.

130 Complicating the picture further was the additional finding in Dzepina et al. (2011) that if
131 the VBS with multi-generational aging was applied to VOCs following Tsimpidi et al. (2010),
132 then all the SOA mass could be successfully predicted without considering P-S/IVOCs. A similar
133 finding was observed in Tsimpidi et al. (2010) wherein the inclusion of P-S/IVOCs and an
134 “aging VBS” treatment of VOC oxidation worsened over-prediction in the model during the

135 afternoon. Thus, the relative importance of P-S/IVOCs versus VOCs in urban SOA production
136 remains very uncertain. More generally, robust model/measurement closure – in which SOA
137 chemistry is accurately represented – is an important step towards implementing effective
138 particulate matter pollution controls in urban areas.

139 Here we compare the results of a constrained SOA box model against measurements
140 carried out at the Pasadena ground site during the California Research at the Nexus of Air
141 Quality and Climate Change (CalNex) campaign. The use of a box model allows multiple state-
142 of-the-art parameterizations to be tested. Once constrained by measurements, the box model
143 facilitates the improved source apportionment of SOA in the Los Angeles Metropolitan Area. In
144 particular, the amount of SOA formed from different precursors is quantitatively evaluated. The
145 importance of diesel versus gasoline emissions as sources of SOA precursors – a topic that has
146 received much recent interest – is discussed as well (Bahreini et al., 2012; Gentner et al., 2012;
147 Hayes et al., 2013; Ensberg et al., 2014). Results are also compared to those of the 3-D WRF-
148 CMAQ model. The CalNex field campaign, which took place in Spring/Summer 2010, provides
149 a unique data set for evaluating [gas-phase](#) SOA models because of, in part, the large scope of the
150 campaign, and the generally clear-sky conditions during the campaign that limited the effects of
151 cloud chemistry. Specifically at the Pasadena ground site, which operated from May 15 2010 to
152 June 15 2010, there were over 70 gas and particle phase measurements including cutting-edge
153 techniques that provide new insights into SOA sources and chemistry. For example, highly time
154 resolved ^{14}C measurements with 3 – 4 h resolution are utilized in this work, whereas typically 12
155 h or lower resolution has been reported (Zotter et al., 2014). By comparing the CalNex dataset to
156 recently proposed SOA models, the research described below aims to evaluate recently proposed
157 SOA models and assess the importance of different SOA sources and formation pathways.

158

159 **2. Modeling methods**

160 **2.1. Pasadena ground site meteorology**

161 An overview of the CalNex study has been recently published by Ryerson et al. (2013).
162 The location and meteorology of the Pasadena ground site has been described in detail
163 previously (Washenfelder et al., 2011; Hayes et al., 2013). Briefly, the site was located in the
164 Caltech campus about 18 km northeast of downtown Los Angeles (34.1406 N, 118.1225 W).

165 Pasadena lies within the South Coast Air Basin (SoCAB) and the Los Angeles metropolitan area.
166 The prevailing wind direction during daytime in Pasadena was from the southwest, which
167 brought air masses from the Santa Monica and San Pedro bays through Los Angeles to Pasadena.
168 Thus, Pasadena during the daytime is predominately a receptor site for pollution emitted in the
169 western Los Angeles metropolitan area that is then advected over a period of several hours
170 (about 3 – 5 h). While more local emissions and background concentrations of atmospheric
171 species must influence the site, the diurnal cycles of many primary species with anthropogenic
172 sources (e.g. CO, black carbon (BC), and benzene) appear to be dominated by advection of
173 pollution from the southwest. Specifically, CO, BC, and benzene concentrations display strong
174 peaks around noontime as shown in Figure 2 of Hayes et al. (2013), which is due to a transport
175 time of several hours until the emissions from the morning rush hour arrive in Pasadena. At
176 nighttime, winds were weak and were most frequently from the southwest or southeast, which is
177 illustrated in the supporting information (Figure A-2) of Hayes et al. (2013). The site was
178 influenced at that time by more local emissions than by advection from downtown Los Angeles.
179 Aged emissions from the prior daytime may have influenced the site as well during nighttime.

180

181 **2.2. SOA box model**

182 The models in this work are summarized in Table 2. The box model used here accounts
183 for SOA formed from gas-phase oxidation of two sets of precursors: (1) VOCs, and (2) P-
184 S/IVOCs. Also included in the total model SOA is background SOA (BG-SOA), with a constant
185 concentration of $2.1 \mu\text{g m}^{-3}$ that is derived from observations as described later in Section 2.4.
186 BG-SOA is considered non-volatile in the model, which is consistent with observations that very
187 aged SOA has low volatility (Cappa and Jimenez, 2010). For the remainder of the SOA the
188 equilibrium partitioning between the particle and gas-phases is calculated using the
189 reformulation of Pankow Theory by Donahue et al. (2006). The particle-phase fraction of species
190 i , ξ_i , is calculated using its effective saturation concentration, C_i^* , and the total concentration of
191 the organic material available for partitioning, $[OA]$.

192

$$\xi_i = \left(1 + \frac{C_i^*}{[OA]}\right)^{-1} ; [OA] = \sum_i [SVOC]_i \xi_i \quad (1)$$

194

195 We note that there is ongoing scientific research examining if OA adopts a liquid or solid/glassy
 196 phase with potentially slow diffusion properties, and the conditions that result in equilibrium or
 197 kinetically-limited partitioning are not yet clear (e.g. Cappa and Wilson, 2011; Perraud et al.,
 198 2012). For the purpose of this study however, field measurements from CalNex strongly suggest
 199 that organic aerosols undergo equilibrium partitioning in Pasadena (Zhang et al., 2012). In
 200 particular, for water-soluble organic carbon, a surrogate for SOA, the partitioning coefficient was
 201 observed to be correlated with the OA mass. A similar observation was made at a rural site in
 202 Colorado, USA, and the lack of kinetic limitations to equilibrium may be attributable to the
 203 higher ambient relative humidity, mostly greater than 30%, in both Pasadena and Colorado
 204 compared to some studies that have reported kinetic limitations (Yatavelli et al., 2014).
 205 Furthermore, we note that the diurnally averaged relative humidity in Pasadena was always
 206 greater than 60%, which laboratory studies have suggested is above the ~30% threshold
 207 wherein particles form liquid phases (Renbaum-Wolff et al., 2013).

208 V-SOA in the box model includes products from the oxidation of 46 VOCs, and the V-
 209 SOA mass is distributed into a 4-bin VBS as shown Figure 1 ($C^*=1, 10, 100, \text{ or } 1000 \mu\text{g m}^{-3}$).
 210 Furthermore, a table with the names of each VOC as well as the relevant model parameters is
 211 provided in the supporting information (Table SI-1). The reaction rates for most of the VOCs are
 212 taken from Atkinson and Arey (2003) and, when not available there, Carter (2010). Three
 213 terpene compounds (α -pinene, β -pinene, and limonene) were lumped for this model, and the rate
 214 constant of this lumped precursor species is the weighted average – by ambient concentrations –
 215 of the individual rate constants (Atkinson and Arey, 2003). In addition, the rates for naphthalene,
 216 1-methylnaphthalene, and 2-methylnaphthalene oxidation are taken from Chan et al. (2009). The
 217 SOA yields for the VOCs are taken from Tsimpidi et al. (2010). For naphthalene and the
 218 methylnaphthalenes the yields are from data presented in Chan et al. (2009), which have been re-
 219 fitted to obtain yields for the 4-bin VBS utilized in this work. V-SOA is also allowed to ‘age’
 220 after the initial reaction, and the subsequent gas-phase oxidation (with a rate constant of 10^{-11}
 221 $\text{cm}^3 \text{ molec.}^{-1} \text{ s}^{-1}$, which was erroneously reported as 4 times higher in Tsimpidi et al. (2010))

222 leads to a 10× decrease in volatility as well as a 7.5% increase in mass due to added oxygen for
223 each generation. This parameterization for V-SOA is abbreviated as “TSI” in the text.

224 It is possible that the SOA yields used for V-SOA, which are based on the chamber
225 experiment literature, are several-fold too low due to, for example, losses of gas-phase species to
226 chamber walls (Matsunaga and Ziemann, 2010; Zhang et al., 2014). To investigate this
227 possibility a model variation – named “~~ROB~~+4xV” – is run wherein the SOA yields from
228 aromatics are increased by a factor of four, based on recent chamber studies in which higher
229 concentrations of aerosol seed were utilized in order to suppress losses to chamber walls, and an
230 upper limit of a factor of 4 increase in V-SOA yields was estimated (Zhang et al., 2014). The
231 multi-generation aging of secondary species produced from VOCs is turned off in this variation,
232 since otherwise the SOA yields would reach extremely unrealistic levels (~400%).

233 SOA from P-S/IVOCs (SI-SOA) is simulated utilizing three different parameter sets. No
234 duplication of precursors is expected between the Tsimpidi et al. (2010) parameterization and the
235 three P-S/IVOCs parameterizations, with the possible exception of the naphthalenes (Robinson et
236 al., 2007; Dzepina et al., 2009; Dzepina et al., 2011). However, since the naphthalenes contribute
237 a very small amount to the total SOA mass (see below), the impact of double-counting their SOA
238 contribution is negligible. The first two P-S/IVOCs parameterizations are from Robinson et al.
239 (2007), hereinafter “ROB”, and an alternate set published by Grieshop et al. (2009), hereinafter
240 “GRI”. The differences between the two parameterizations are highlighted in Figure 1. When
241 compared to ROB, primary and secondary species in GRI have a lower gas-phase reactivity
242 (2×10^{-11} versus 4×10^{-11} $\text{cm}^3 \text{ molec}^{-1} \text{ s}^{-1}$), a larger decrease in volatility per oxidation step (two
243 orders of magnitude versus one), and more oxygen mass added to the products (40% versus 7.5%
244 of the precursor mass). Furthermore, there are differences in the assumed enthalpies of
245 vaporization, ΔH_{vap} , and molecular weights. Details of both parameterizations are given in Table
246 SI-2 in the supporting information.

247 The third parameterization utilized for SI-SOA is that published by Pye and Seinfeld
248 (2010), hereinafter “PYE”, which is also illustrated in Figure 1. In PYE the SOA from primary
249 SVOCs and primary IVOCs follow different treatments. The primary SVOCs emitted are
250 represented by two lumped species with $C^*=20$ and $1646 \mu\text{g m}^{-3}$ and relative concentrations of
251 0.51 and 0.49, respectively. The gas phase reactivity ($2 \times 10^{-11} \text{ cm}^3 \text{ molec}^{-1} \text{ s}^{-1}$) and decrease in

252 volatility per oxidation step (two orders of magnitude) are identical to GRI. However, only one
253 oxidation step is allowed in PYE. The oxygen mass added to the products is 50% of the
254 precursor mass, which is higher than that for ROB and GRI. Another difference in PYE is the
255 enthalpy of vaporization for all organic species, which is 42 kJ/mol. Lastly, the molecular weight
256 utilized here is 250 g mol^{-1} , the same as ROB, although this parameter is not specified in Pye and
257 Seinfeld (2010). In PYE also the concentration of SOA from primary IVOCs is estimated by
258 scaling-up the concentration of SOA from naphthalene by a factor of 66.

259 Heterogeneous uptake of glyoxal onto aerosols can be a relevant source of SOA under
260 some conditions (Volkamer et al., 2007; Dzepina et al., 2009). Previously published work on the
261 glyoxal budget for CalNex indicates that this compound contributes only a small fraction of the
262 SOA mass in the LA basin, however (Washenfelder et al., 2011; Knote et al., 2014b), and we do
263 not consider it further in this study. In Pasadena, the urban SOA peaked in the afternoons, which
264 were generally clear and sunny during the campaign. This observation is consistent with the
265 conclusion that reactions occurring in clouds did not play a major role in SOA production during
266 CalNex. In addition, a comparison of $\text{OA}/\Delta\text{CO}$ for three days that were cloudy against the
267 remainder of the campaign shows no apparent difference in the magnitude of the ratio or its
268 evolution with photochemical age (Figure SI-1), which further supports the conclusion that SOA
269 production from clouds can be neglected in this study.

270 The design of the model used here includes several more elements that are general for V-
271 SOA and SI-SOA. Only oxidation by hydroxyl radical ($\bullet\text{OH}$) is considered since in urban
272 regions other oxidants such as ozone, nitrate radical, and chlorine radical are expected to be
273 minor contributors to SOA formation from urban VOCs (Dzepina et al., 2009; Dzepina et al.,
274 2011; Hayes et al., 2013). Additionally, the model is run using “high- NO_x conditions,” which is
275 consistent with previously calculated branching ratios for the $\text{RO}_2 + \text{NO}$, $\text{RO}_2 + \text{HO}_2$, and $\text{RO}_2 +$
276 RO_2 reactions (Hayes et al., 2013) and the dominance of the $\text{RO}_2 + \text{NO}$ pathway. The primary
277 and secondary species are assumed to mix into a single organic phase. This assumption is based
278 on observations made off the coast of California that SOA condenses on primary particles (e.g.,
279 BC and POA) as indicated by the similar size distributions for these species across a range of
280 photochemical ages (Cappa et al., 2012). In addition, the organic phase is taken to be separate
281 from the inorganic phases, which is consistent with the relatively low O:C values observed

282 during CalNex (Hayes et al., 2013) and previous studies demonstrating that organic/inorganic
283 phase separation occurs when O:C is less than 0.7 (Bertram et al., 2011). It should be noted that
284 this statement holds true even after applying the updated calibration for AMS O:C (Canagaratna
285 et al., 2015).

286 The temperature dependence of C^* is calculated with the Clausius-Clapeyron equation.

287

$$288 \quad C_i^* = C_{i,o}^* \frac{T_0}{T} \exp \left[\frac{\Delta H_{vap}}{R} \left(\frac{1}{T_0} - \frac{1}{T} \right) \right] \quad (2)$$

289

290 Where $C_{i,o}^*$ is the effective saturation concentration of condensable compound i at the reference
291 temperature T_0 (K), and R is the ideal gas constant. The ambient temperature, T , was taken to be
292 18°C, which represents the average campaign temperature during CalNex. A sensitivity test
293 exhibited less than a 4% change in predicted mass at a given time-of-day when using 14°C and
294 24°C, which are the minimum and maximum temperatures for the diurnal cycle. The error in
295 predicted mass over this temperature range is small compared to other uncertainties in SOA
296 modeling, and therefore the use of a constant temperature of 18°C to calculate C^* should
297 introduce negligible errors.

298

299 **2.3. Model set-up**

300 This work utilizes a box approach wherein the model calculates the evolution of organic
301 species in an air parcel as it undergoes photochemical aging. A schematic of the model set-up is
302 shown in Figure 2. The calculation is run 24 times to predict the average diurnal cycle for the
303 entire campaign (15 May – 15 June). For each of the 24 repetitions, the calculation always starts
304 at hour zero and then runs to 12 h of photochemical aging (Panel 2). Next, the model output at
305 the same photochemical age as that observed at the Pasadena ground site for the given time-of-
306 day is saved for comparison against measurements (Panel 3). The initial concentrations of VOCs
307 in the air parcel are calculated by multiplying the background-subtracted CO concentrations
308 measured at Pasadena by the emission ratios, $\Delta\text{VOC}/\Delta\text{CO}$, previously determined for CalNex,
309 which are consistent with those for other US urban areas (Warneke et al., 2007; Borbon et al.,

310 2013) (Panel 1). CO is an inert tracer of combustion emissions over these timescales and its
311 formation from VOCs is very minor as well (Griffin et al., 2007). The CO background level
312 represents the amount present from continental-scale transport and for which the co-emitted
313 organic species have been lost by deposition (e.g. DeCarlo et al., 2010). The background was
314 determined by examining CO measurements taken aboard the NOAA WP-3D aircraft off the Los
315 Angeles coastline at altitudes less than 200 m as described in our previous paper (Hayes et al.,
316 2013). Given that the model is set-up to predict the mean diurnal cycle of SOA during the entire
317 CalNex-Pasadena measurement period, the mean diurnal cycle of the CO concentration is used
318 for the calculation of the emissions. An important advantage of using CO as a conserved urban
319 emissions tracer is that dilution of emissions in the air parcel is implicitly included in the model,
320 since the reductions in CO concentration will lead to lower calculated initial precursor
321 concentrations in that air parcel.

322 The biogenic VOCs are not expected to be emitted proportionally with CO, and therefore
323 the approach described in the previous paragraph cannot be used to specify the biogenic VOC
324 emissions. Rather, ~~t~~The emissions of biogenic VOCs were adjusted empirically to match the
325 observed concentrations of isoprene and terpenes, after accounting for anthropogenic isoprene
326 using $\Delta(\text{isoprene})/\Delta\text{CO}$ (Borbon et al., 2013). Only ~4% of the daily average isoprene is from
327 anthropogenic sources. In addition, the diurnal profile of emissions was assumed to be
328 proportional to ambient temperature.

329 The model consistency with the VOC measurements, including for biogenic VOCs, is
330 evaluated by comparing the measured and modeled diurnal cycles. Some of ~~t~~The cycles
331 compared are given in Figure SI-2 as an example. It is observed that the model is generally
332 consistent with the VOC measurements.

333 For naphthalene and its analogs, emission ratios are not available in the literature, to our
334 knowledge. To obtain the emission ratios the concentrations of the polycyclic aromatic
335 hydrocarbons were plotted versus CO, and a linear orthogonal distance regression (ODR)
336 analysis was carried out. The data were filtered and include only periods from 00:00 – 06:00
337 (local time) to minimize depletion by photochemical processing (Figure SI-3). The slope from
338 the regression analysis was then used as the emission ratio. However, as observed in Figure SI-3,
339 the diurnal cycles for naphthalene and its analogs are not well-reproduced by the model during

340 the daytime when using the early morning emission ratios. The sampling of these compounds
341 was performed on a tar roof, and it is possible that the local concentrations in the vicinity of roof
342 may be elevated during daytime due to volatilization of the roofing tar and not representative of
343 concentrations throughout the Los Angeles basin. The naphthalene and methylnaphthalene
344 concentrations are well correlated with temperature. However, it is also possible that the
345 volatilization occurs over a larger city scale, and thus a variation of the model is run wherein the
346 emission ratios are changed empirically along the diurnal cycle so that the model reproduces the
347 measured diurnal cycle for each speciated naphthalene (Figure SI-3). The increases in emissions
348 range between 1 and 3.5 times the original value, and the implications for SOA are discussed in
349 Section 3.1.3.

350 The calculation of the initial P-S/IVOC concentrations requires a somewhat different
351 procedure compared to the VOCs. Instead, the amount of initially emitted POA is calculated
352 from measured $\Delta\text{POA}/\Delta\text{CO}$ ratios and the measured CO concentration in Pasadena. Then the
353 total concentration of P-S/IVOCs is set so that the particle-phase P-S/IVOC concentration
354 matches the amount of initially emitted POA, while constraining the volatility distribution to that
355 of the corresponding parameterization, as done in previous studies (e.g. Dzepina et al., 2009).

356 The model consistency with respect to the POA measurement is shown in Figure SI-2.
357 The comparison for POA is adequate, and a linear ODR analysis yields a slope of 1.01 ($R =$
358 0.76) when the GRI+TSI parameterization is used. Of these three model variants, PYE+TSI
359 shows a larger positive bias. This is likely due to the relatively large amount of primary SVOCs
360 placed in the $C^*=20$ bin compared to ROB+TSI and GRI+TSI, which will result in more
361 partitioning to the particulate phase as the total OA mass is increased (e.g. by SOA formation)

362 The initial VOCs and P-S/IVOCs are then oxidized in the air parcel. The aging of the air
363 parcel is simulated separately 24 times with each simulation using measured parameters (e.g.
364 ΔCO , photochemical age, POA) corresponding to one hour during the mean diurnal cycle.
365 Following Dzepina et al. (2009) the evolution of the different compounds in each of the 24 aging
366 simulations is calculated by discretizing the rate equations using Euler's method.

367 The photochemical age of the urban emissions at each time of day is determined from the
368 ratio of 1,2,4-trimethylbenzene to benzene as described previously (Parrish et al., 2007; Hayes et
369 al., 2013). We note that the photochemical age estimated from NO_y/NO_x is very similar (Hayes

370 et al., 2013), which is consistent with previous results from Mexico City for ages shorter than 1
371 day (C. A. Cantrell, Univ. of Colorado, personal communication, 2014). There are three
372 important considerations that must be evaluated when using VOC concentration ratios as
373 photochemical clocks.

374 First, trimethylbenzene and benzene are predominately from anthropogenic sources, and
375 thus the photochemical clock only applies to the evolution of anthropogenic emissions. Previous
376 work by Washenfelder et al. (2011) estimated that most biogenic VOCs were emitted mostly in
377 the last quarter of the trajectory of the air parcel arriving at Pasadena at 16:00 PDT. This estimate
378 was based on the vegetation coverage observed in visible satellite images of the upwind areas, as
379 well as on the ratio of isoprene to its first-generation products (methyl vinyl ketone and
380 methacrolein). However, in this work, the photochemical age for biogenic VOCs is kept the
381 same as for the anthropogenic VOCs. This approach will overestimate the amount of
382 photochemical aging – and the SOA from in-basin biogenic emissions – during daytime. The
383 modeled biogenic SOA should thus be considered an upper limit. ~~The emissions of biogenic~~
384 ~~VOCs were adjusted empirically to match the observed concentrations of isoprene and terpenes,~~
385 ~~after accounting for anthropogenic isoprene using $\Delta(\text{isoprene})/\Delta\text{CO}$ (Borbon et al., 2013). Only~~
386 ~~4% of the daily average isoprene is from anthropogenic sources.~~ As discussed below, the
387 amount of SOA from in-basin biogenic VOCs is very small. Thus, our SOA model results are not
388 sensitive to the details of how SOA from biogenic VOCs emitted within the LA basin is
389 modeled. We do not include oxidation of biogenic VOCs by O_3 or NO_3 in the box model, but
390 these oxidants have only a minor role in SOA formation during the daytime when the peak for
391 in-basin SOA concentration is observed. In particular, given the measured concentrations of
392 oxidants (Hayes et al., 2013), oxidation of isoprene and terpenes by $\bullet\text{OH}$ is 37 and 5 times faster
393 on average, respectively, than oxidation by O_3 during daytime.

394 The second consideration is that the purpose of using the ratio of VOC concentrations is
395 to determine the $\bullet\text{OH}$ exposure for the air mass at the Pasadena site. ($\bullet\text{OH}$ exposure is the
396 concentration integrated over time for an air parcel.) While the $\bullet\text{OH}$ exposure for the site is
397 therefore well-constrained, the actual $\bullet\text{OH}$ concentration in the modeled air parcel as a function
398 of time is not as well-constrained. Thus, the photochemical ages used here (Figure 3) are
399 calculated using an average $\bullet\text{OH}$ concentration of $1.5 \times 10^6 \text{ molec cm}^{-3}$, as described in our

400 previous work (Hayes et al., 2013), and. ~~The model is run with the same concentration, which is~~
401 ~~necessary to match the model and observed OH exposure. (•OH exposure is the concentration~~
402 ~~integrated over time for an air parcel.)~~ Insofar as the model produces the same •OH exposure as
403 determined from measurements, which is always the case in this modeling study, the actual
404 concentration of •OH used in the model is not expected to substantially influence the results. In
405 other words, while the concentration •OH in the model is assumed to be 1.5×10^6 molec cm^{-3} , the
406 integral of the •OH concentration over time is constrained by the observed VOCs ratios. Thus As
407 expected, in the middle of the day the photochemical age will be longer than the transport age,
408 and the opposite will be true during periods with low ambient •OH.

409 Third, photochemical age is a quantity developed as a metric for parcels of air arriving at
410 a remote receptor site, and it is derived by assuming that the parcel is decoupled from fresh
411 emissions as it is transported (Kleinman et al., 2007; Parrish et al., 2007). However, Pasadena is
412 not a remote receptor site, and it is impacted by pollution that has been emitted recently as well
413 as transported from more distant locations. The error in the calculated photochemical age that
414 results from the mixing of nearby and far sources is evaluated in our previous work, and it may
415 lead to underestimation of the actual photochemical age by ~10% (Hayes et al., 2013), which is
416 relatively minor compared to the uncertainty in the OA measurement of $\pm 30\%$ (Middlebrook et
417 al., 2012) and the possible biases in the different SOA parameterizations.

418

419 **2.4. Model/measurement comparisons**

420 The model is compared against the average diurnal cycles of various OA properties (e.g.
421 concentration, O:C). The measurements utilized in this study are summarized in Table 3. In
422 previous work the concentrations of five different OA components were determined using
423 positive matrix factorization (PMF) of aerosol mass spectrometer (AMS) data, and the diurnal
424 cycles of these components are shown in Figure 3 (Hayes et al., 2013). Hydrocarbon-like organic
425 aerosol (HOA) and cooking-influenced organic aerosol (CIOA) are both thought to be dominated
426 by POA. As discussed in Hayes et al. (2013), HOA is dominated by vehicle combustion
427 emissions, and the CIOA is dominated by cooking sources. However, for the purpose of running
428 the SOA model, HOA and CIOA are not treated separately, and instead their summed mass

429 concentrations are used as the POA concentration. It should be noted however that the amount of
430 SOA from HOA or CIOA associated P-S/IVOCs can still be calculated under certain
431 assumptions as discussed in Section 3.1.2 below. Low volatility oxygenated organic aerosol
432 (LV-OOA) is a surrogate for highly aged secondary organic aerosol, and it displays a flat diurnal
433 profile. Furthermore, recent ^{14}C measurements show that this component is largely composed of
434 non-fossil carbon (Zotter et al., 2014). Both of these observations indicate that LV-OOA is
435 transported into the Los Angeles Basin (Hayes et al., 2013).

436 Results from 3-D WRF-Chem simulations were also used to evaluate the concentration of
437 BG-SOA. These simulations determined the BG-SOA by removing all the emissions in the Los
438 Angeles region as shown in Figure SI-4, and it was observed that there are both biogenic and
439 anthropogenic emissions in California that contribute to the background OA. In addition,
440 background marine OA is thought to be very low during the CalNex measurement period, since
441 concentrations of OA were less than $0.2 \mu\text{g m}^{-3}$ over the open ocean west of California for
442 regions with low pollution influence (P. K. Quinn, NOAA, personal communication, 2012). As
443 shown in Figure 3B, the background SOA concentration from the WRF-Chem simulation is
444 similar to the concentration of LV-OOA. Given these observations as well as the ^{14}C results
445 discussed in the previous paragraph, we use the LV-OOA component to constrain the amount of
446 BG-SOA, and specifically, set the amount of BG-SOA to be the minimum of LV-OOA observed
447 in the diurnal cycle ($2.1 \mu\text{g m}^{-3}$). [Heo et al. \(2015\) recently concluded that the background SOA
448 in the LA basin has an important component from biogenic emissions over the Central Valley,
449 which is consistent with our results.](#)

450 In contrast, semi-volatile oxygenated organic aerosol (SV-OOA) displays a distinct
451 diurnal profile that peaks at a similar time as photochemical age, which is consistent with this
452 component being a proxy for freshly formed SOA from urban emissions. The ^{14}C measurements
453 also indicate that SV-OOA is predominately, 71% ($\pm 3\%$), composed of fossil carbon. (Note: to
454 obtain this percentage it is assumed that the OC/OM ratio is the same for fossil and non-fossil
455 SV-OOA.) As described above, the box model designed here is specifically focused on SOA
456 formation from precursors emitted within the Los Angeles basin, and the ^{14}C measurements and
457 diurnal cycle strongly indicate that SV-OOA concentration is a better surrogate for total urban
458 SOA than the total OOA concentration. Lastly, there is a fifth component displayed in Figure 3B,

459 local organic aerosol (LOA) of primary origin and of uncertain sources, but this component
460 comprises only ~5% of the aerosol mass. It is thought to be emitted very close to the site based
461 on its very rapid time variations, and thus any co-emitted VOCs or S/IVOCs would have very
462 little time to react and form SOA. Therefore, LOA is not considered further in this modeling
463 study.

464 In principle, the box model could be run for multiple individual days. However, some
465 datasets and published results used in this study are not available with sufficient time resolution
466 for such an approach. In particular, the thermal desorption gas chromatograph mass spectrometry
467 analysis for naphthalenes required adsorbent tube filter samples that were composited over
468 several days. In addition, both the apportionment of the SV-OOA and LV-OOA components
469 between fossil and non-fossil sources (Zotter et al., 2014) as well as the analysis of the diesel
470 fraction of OOA (Hayes et al., 2013) required analyzing datasets from multiple days as a single
471 ensemble. To facilitate incorporating these datasets and published results into this study, we have
472 chosen to run the box model so that it simulates the average diurnal cycle during the campaign.
473 The measurements used here (Table 3) all had excellent coverage during the CalNex campaign,
474 with each instrument reporting data for more than 75% of the total campaign duration. Thus, the
475 measurements are expected to be representative of conditions during the campaign. An exception
476 is the ^{14}C measurements, which were carried out on filters collected over 7 days. This limited
477 sampling period is due to the time and resource intensive nature of the ^{14}C measurements (Zotter
478 et al., 2014). In particular, the dates that the filters were collected were 30 May as well as 3, 4, 5,
479 6, 13, and 14 June 2010. Thus, these filters are more representative of the second half of the
480 campaign that was more strongly influenced by pollution from the basin, compared to the first
481 half of the campaign where regional advection played a more important role (Ryerson et al.,
482 2013). Given the cost of the ^{14}C analyses, these days were chosen on the basis of the larger urban
483 influence determined from the real-time measurements and are therefore better suited to
484 constrain urban sources (the subject of this paper) than if the analyses had been performed on
485 filters from randomly-chosen days. However, it is noted that the relative concentrations of the
486 different components of the OA were similar when averaging the second half of the campaign or
487 the entire campaign: 14% vs. 12% for HOA, 5% vs. 5% for LOA, 12% vs. 17% for COA, 28%
488 vs. 34% for LV-OOA, 40% vs. 34% for SV-OOA. Thus, it appears reasonable to assume that the
489 relative results from the ^{14}C analysis are representative of the entire campaign.

490

491 **2.5. Modeling the SOA oxygen content**

492 To simulate the oxygen-to-carbon ratio (O:C) of total OA, the box model utilizes the
493 measured O:C for HOA, CIOA, and LV-OOA. The O:C values for HOA and CIOA are assumed
494 to be constant because heterogeneous aging of primary aerosols is relatively slow, and thus the
495 O:C should only vary by a relatively small amount [due to this mechanism over the timescales](#)
496 [considered here](#) (Donahue et al., 2013). LV-OOA is predominately composed of aged
497 background OA, and thus its O:C should not vary substantially either. The oxygen and carbon
498 mass from HOA, CIOA, and LV-OOA are then added to the oxygen and carbon mass predicted
499 in the model for freshly formed SOA.

500 The O:C of V-SOA is simulated using a modified version of the approach described in
501 Dzepina et al. (2009). In that previous work the O:C of V-SOA was estimated to be 0.37 and
502 constant. While this estimate is consistent with chamber experiments of aromatic precursors, it is
503 conceptually difficult to reconcile with V-SOA aging wherein successive oxidation reactions are
504 expected to reduce volatility and increase O:C. It is therefore assumed in the box model that O:C
505 increases as follows: $C^* = 1000 \mu\text{g m}^{-3}$, O:C = 0.25; $C^* = 100 \mu\text{g m}^{-3}$, O:C = 0.30, $C^* = 10 \mu\text{g}$
506 m^{-3} ; O:C = 0.40; $C^* = 1 \mu\text{g m}^{-3}$, O:C = 0.60. This O:C distribution is taken from the first-
507 generation distribution of Murphy et al. (2011), and in that work the O:C was simulated in a full
508 2-D VBS and depends on both volatility bin as well as oxidation generation. For the purpose of
509 this study an intermediate approach is used wherein O:C depends on volatility bin only, and the
510 first-generation distribution of Murphy et al. (2011) is applied to all oxidation generations of
511 SOA. We note that only a small amount of V-SOA mass is from multi-generation oxidation (10
512 – 20%) for the relevant model conditions used [for Pasadena](#). Thus, the O:C values predicted here
513 will not be substantially different from a full 2-D VBS treatment.

514 The O:C ratio for SI-SOA is simulated following the approach described in Robinson et
515 al. (2007). Conceptually, with each oxidation step the model adds 1 oxygen atom per 15 carbon
516 atoms for ROB and 5.3 oxygen atoms per 15 carbons for GRI. This oxidation then gives an
517 increase in mass of 7.5% or 40% for ROB and GRI, respectively, as discussed previously. (Note:
518 It is assumed that $H = 2 \times C + 2$, which may not be strictly true, but an error of 1 or 2 hydrogen
519 atoms per carbon does not substantially alter the calculated values for the mass increase.) With

520 this relationship O:C can be calculated for each generation of oxidation, and the OM:OC ratio
521 can be calculated as well using the relationship $OM:OC = 1 + (16/12) \times O:C + (1/12) \times H:C$, in
522 which $H:C = 2 - 0.54 \times O:C$ (Murphy et al., 2011; Hayes et al., 2013; Canagaratna et al., 2015).
523 Then the OM:OC ratio is used to convert the OM mass concentration in each generation bin to
524 OC mass concentration, and the O:C ratio is used to convert the OC mass in each generation bin
525 to O mass concentration. Finally, the O mass and OC mass are each summed and subsequently
526 divided to obtain O:C.

527

528 **2.6. Correction for changes in partitioning due to emissions into a shallower** 529 **boundary layer upwind of Pasadena**~~due to higher OA concentrations upwind of~~ 530 **Pasadena**

531 To account for changes in partitioning due to lower planetary boundary layer (PBL)
532 heights, and thus, increased ~~OA particle~~ concentrations upwind of Pasadena, the concentrations
533 of POA, V-SOA, and SI-SOA are increased upwind of Pasadena beyond the amount already
534 simulated in the model. This correction is necessary because using CO as a conservative tracer of
535 emissions does not account for how ~~particulate concentration~~ the shallow boundary layer over
536 Los Angeles in the morning influences partitioning ~~between the gas and particle phases upwind~~
537 ~~of Pasadena~~. Specifically, during the afternoon Pasadena is a receptor site for pollution from
538 downtown Los Angeles that was generally emitted into a shallower boundary layer during the
539 morning. The reduced vertical dilution will lead to higher concentrations of POA as well as any
540 urban SOA formed, which in turn leads to higher partitioning to the particle phase and less gas
541 phase oxidation of primary and secondary S/IVOCs.

542 The correction of the partitioning mass is estimated using three different methods
543 depending on the time-of-day. First, for air parcels measured at 00:00 – 07:00 local time when
544 the PBL height is essentially constant for an extended period and emissions are dominated by
545 local sources (Hayes et al., 2013), no correction needs to be made. Second, for air parcels
546 measured between 07:00 – 16:00 when the PBL is increasing as the air parcels are advected, a
547 correction is applied that assumes the PBL increases linearly from the height measured in the
548 early morning hours to the height measured for a given time of day. Third, for air parcels after

549 16:00, it is assumed that a residual layer aloft is decoupled from the ground after 16:00, resulting
550 in no subsequent dilution.

551 The correction for the partitioning calculation described in the previous paragraph is an
552 approximation, and two sensitivity studies are carried out to estimate the magnitude of the
553 possible errors introduced by this approximation. The first study follows the approach described
554 above, except that instead of linearly increasing the partitioning mass upwind of Pasadena the
555 correction follows a step-function and increases the partitioning mass to its maximum value
556 immediately upwind of the ground site. This test should overestimate the amount of partitioning
557 to the particle-phase, since such a dramatic change in PBL height is not expected. The second
558 sensitivity study simply applies no correction factor to the partitioning mass, and thus it
559 underestimates the partitioning to the particle-phase. For the model runs with the ROB+TSI and
560 GRI+TSI parameterizations the resulting changes in average predicted mass for the sensitivity
561 studies are +4/-12% and +6/-7%, respectively. These changes are small, which indicates that the
562 description of the boundary layer dilution does not have a major influence on the results.

563

564 **2.7. WRF-CMAQ model runs**

565 The Community Multiscale Air-Quality Model (WRF-CMAQ) version 5.0.1
566 (<https://www.cmascenter.org/cmaq/>) was applied with 4 km horizontal grid resolution and 34
567 vertical layers extending from the surface (layer 1 height ~38 m) to 50 mb for the time period
568 matching the CalNex field campaign. Aqueous phase chemistry includes oxidation of sulfur and
569 methylglyoxal (Carlton et al., 2008; Sarwar et al., 2013), gas phase chemistry is based on Carbon-
570 Bond 05 with updates to toluene reactions (CB05-TU) (Yarwood, 2010), and inorganic
571 chemistry is based on the ISORROPIA II thermodynamic model (Fountoukis and Nenes, 2007).
572 WRF-CMAQ estimates SOA yields from VOC precursors including isoprene, monoterpenes,
573 sesquiterpenes, xylenes, toluene, benzene, and methylglyoxal (Carlton et al., 2010). Note that
574 WRF-CMAQ contains the SOA precursor species alkanes and glyoxal, but these are not explicit
575 species in the CB05-TU gas phase mechanism (e.g., alkanes are mapped to “PAR”, or paraffins).
576 SOA species oligomerize to non-volatile organic carbon grouped by anthropogenic and biogenic
577 origin (Carlton et al., 2010).

578 The Weather Research and Forecasting model (WRF), Advanced Research WRF core
579 (ARW) version 3.1 (Skamarock et al., 2008) was used to generate gridded meteorological fields
580 used for input to WRF-CMAQ and the emissions model. Surface variables, flow patterns, and
581 daytime mixing layer heights are generally well characterized during this time period (Baker et
582 al., 2013). Hourly solar radiation and surface layer temperature estimated by the WRF model are
583 used as input for the Biogenic Emission Inventory System (BEIS) version 3.14 to estimate
584 hourly speciated VOC and NO_x emissions (Carlton and Baker, 2011).

585 Stationary point source emissions are based on continuous emissions monitor (CEM) data
586 for 2010 where available and otherwise the 2008 version 2 National Emission Inventory (NEI).
587 Area source emissions are also based on the 2008 version 2 NEI. Mobile sector (on-road and off-
588 road) emissions are interpolated between 2007 and 2011 totals provided by the California Air
589 Resources Board. Emissions from other areas of the United States and other countries are
590 included through time and space variant lateral boundary inflow. Hourly boundary inflow
591 concentrations are taken from a coarser WRF-CMAQ simulation covering the continental United
592 States that used inflow estimates from a global GEOS-CHEM (version 8.03.02) model
593 (<http://acmg.seas.harvard.edu/geos/>) simulation. Additional details regarding model setup and
594 evaluation are provided elsewhere (Kelly et al., 2014).

595

596 **2.8. WRF-Chem model runs**

597 Weather Research and Forecasting Model coupled to Chemistry (WRF-Chem) is a fully
598 coupled meteorology-chemistry model. WRF-Chem simulations were performed for May and
599 June 2010 on a 12 km resolution domain, which covers a large part of the western United States.
600 The model simulations include meteorological, gas, and aerosol phase chemical processes. The
601 SOA scheme used in this study is based on the VBS approach. The SOA parameterization and
602 other model parameterizations are described in detail by Ahmadov et al. (2012). Here the main
603 objective of the WRF-Chem simulation was to estimate the OA contribution of the emission
604 sources located upwind of the Los Angeles basin. Thus, all the anthropogenic emissions and
605 biogenic VOC fluxes were set to zero over an area of 60 x 72 km covering the Los Angeles basin
606 (Figure SI-4) in our simulation. The WRF-Chem simulated OA concentrations for the Pasadena
607 site therefore provide an estimate of the BG-OA at this site.

608

609 3. Results and discussion

610 3.1. Modeling urban SOA mass concentration

611 3.1.1. Urban SOA concentration: model versus measurement comparisons

612 In Figure 4 the diurnal cycles of SV-OOA and urban SOA are shown. For all the model
613 variations, the model V-SOA (light blue area) is substantially smaller than the observed SV-
614 OOA concentrations (solid black line), even though the additional partitioning mass of SI-SOA
615 is available for all model runs. ~~It is possible that the SOA yields used for V-SOA, which are
616 based on the chamber experiment literature, are several fold too low due to, for example, losses
617 of gas phase species to chamber walls. To investigate this possibility a model variation named
618 "ROB+4xV" is run wherein the SOA yields from aromatics are increased by a factor of four,
619 based on recent chamber studies in which higher concentrations of aerosol seed were utilized in
620 order to suppress losses to chamber walls, and an upper limit of a factor of 4 increase in V-SOA
621 yields was estimated (Zhang et al., 2014). The multi-generation aging of secondary species
622 produced from VOCs is turned off in this variation. The result for ROB+4xV is shown in Figure~~
623 4. Even in ~~theis~~ model variation ROB+4xV where the V-SOA concentrations are substantially
624 higher due to the higher VOC yields used, additional SOA precursors must be included to
625 achieve model/measurement closure. This result is also true despite the inclusion of multi-
626 generation V-SOA aging in ROB+TSI, GRI+TSI, and PYE+TSI, which increases the amount of
627 SOA from VOCs to levels far beyond those observed in chambers, although over longer
628 timescales than for the 4xV case. Previous work modeling SOA in Mexico City showed that
629 either V-SOA aging or SI-SOA must be included in models to match observed SOA
630 concentrations, but the inclusion of both resulted in an overprediction (Tsimpidi et al., 2010;
631 Dzepina et al., 2011). In this study, the inclusion of aging only increases the concentration of V-
632 SOA by 10 – 20% depending on the time of day due to the relatively low experimental
633 photochemical ages. Thus, by testing models of SOA formation at short ages, our case study
634 points towards the importance of additional SOA precursors such as P-S/IVOCs. Specifically,
635 the contribution to total SOA from P-S/IVOCs in the box model is 65-75% (ROB+TSI), 80-87%
636 (GRI+TSI), 80-92% (PYE+TSI), and 44-51% (ROB+4xV). The range indicates the variation in
637 the contribution with the time-of-day. Thus, only in the ROB+4xV model variation is the

638 estimated contribution to SOA from VOCs generally larger than or equal to that from the P-
639 S/IVOCs. We note however these percentages include only the urban SOA and not the
640 background OA, which is likely also SOA as discussed above.

641 When comparing the four parameterizations for SOA formation, it is apparent that the
642 GRI+TSI and ROB+4xV variations best reproduce the observations. The predicted SOA mass
643 using GRI+TSI lies within the measurement uncertainty most of the day. In contrast, the
644 ROB+TSI variation does not produce high enough concentrations of SOA, and the model is
645 consistently lower than the measurements even after considering the measurement uncertainties.
646 The PYE+TSI variation tends to over predict SOA concentrations especially at nighttime and in
647 the morning, and also exhibits larger discrepancies with respect to measured POA concentrations
648 (Figure SI-2). Finally, the performance of the ROB+4xV variation is similar to GRI+TSI,
649 highlighting the uncertainties about the dominant SOA precursors in urban areas (i.e. VOCs vs.
650 P-S/IVOCs).

651 In general, the measurements peak one hour later than the model, which may be due to
652 the simple treatment of sources and transport in the modeled air mass, but the overall correlation
653 is excellent: $R = 0.93 - 0.94$ for ROB+TSI, GRI+TSI, PYE+TSI, and ROB+4xV. This study
654 contrasts with an earlier comparison of the ROB and GRI parameterizations for SI-SOA in
655 Mexico City, which showed that GRI produces more SOA than observed (Dzepina et al., 2011).
656 Although the same modeling method was used to quantify the emissions and properties of P-
657 S/IVOCs in both studies, the sources, composition, and SOA yields of P-S/IVOCs in urban areas
658 are poorly characterized, and differences in those between the two urban areas may explain the
659 differences in model performance for Pasadena and Mexico City.

660 In addition, the effective SOA yields predicted in the box model for P-S/IVOCs can be
661 compared against those determined in previous modeling and smog chamber studies. The
662 effective yield is a function of photochemical aging, and thus for the purpose of this comparison
663 we focus on the effective box model yields for 12:00 – 15:00 when there was a moderate amount
664 of photochemical aging (5 h at an average OH concentration of 1.5×10^6 molecules cm^{-3})
665 comparable to the degree of aging typically achieved in chambers. During this period the
666 effective yields for P-S/IVOCs were 12%, 27%, and 36% for ROB+TSI, GRI+TSI, and
667 PYE+TSI, respectively. Zhao et al. (2014) recently carried out a modeling study of SOA formed

668 in Pasadena that was constrained with an extensive set of IVOC data and found an overall SOA
669 yield for IVOCs of 29%, which falls within the range of effective yields for P-S/IVOCs that are
670 predicted by the box model for the three different parameterizations. Jathar et al. (2014) also
671 recently estimated from chamber studies an effective SOA yield of 10 – 40% for unspiciated
672 organic emissions from combustion sources, which is also consistent with the P-S/IVOC yields
673 from our box model. For reference, the effective yields for the aromatic VOCs m-xylene,
674 toluene, and benzene under high-NO_x conditions in chamber studies range from 4 – 28%
675 depending on the precursor identity and chamber conditions (Ng et al., 2007). Similar chamber
676 studies on 12-carbon alkanes determined effective yields ranging from 11% – 160%, where the
677 highest yield corresponded to a cyclic alkane (Loza et al., 2014). In general, it appears that the
678 effective yields resulting from the box model for the lower photochemical ages used here are
679 similar to those determined from other chamber and modeling studies.

680 It is also possible to compare the predicted IVOC concentrations in the box model versus
681 the concentrations measured by Zhao et al. (2014). The comparison is summarized in Table SI-3
682 of the supporting information. In total, the initial IVOC concentrations in the box model are two
683 times higher compared to those determined from measurements (16 $\mu\text{g m}^{-3}$ versus 8(\pm 1) $\mu\text{g m}^{-3}$).
684 In addition, there is a larger difference for the C* = 10³ bin (2.5 $\mu\text{g m}^{-3}$ versus 0.2(\pm 0.1) $\mu\text{g m}^{-3}$).
685 At the same time, the model used by Zhao et al. to predict urban SOA is lower than the
686 measurements by 50% on the urban scale, whereas as the box model used here does not exhibit
687 such a low bias. Given these differences we have run two sensitivity studies to explore how the
688 model predictions depend on the IVOC emissions that are discussed in the following sections.
689 The first sensitivity study reduces the emission of P-S/IVOCs from cooking emissions to zero
690 (Section 3.1.2), and the second sensitivity study reduces all IVOC emissions by one-half (Section
691 3.1.5). Both of these variations greatly improve the agreement between the modeled and
692 measured IVOC concentrations.

693

694 **3.1.2. Total SOA concentration: fossil vs contemporary carbon**

695 As described above, on average 71(\pm 3)% of the SV-OOA is composed of fossil carbon
696 (Zotter et al., 2014), and it is important to evaluate whether this percentage is consistent with the
697 model results. As shown in Figure 4, the V-SOA from in-basin biogenics is very small, and V-

698 SOA is overwhelmingly from fossil carbon sources since it is dominated by aromatic precursors
699 (see 3.1.3 below) and the main source of aromatic hydrocarbons in the Los Angeles basin is
700 vehicle emissions (Borbon et al., 2013). For SI-SOA, two types of POA, and thus, primary P-
701 S/IVOCs are included in this study. Since HOA is dominated by vehicle emissions, it is most
702 likely composed of fossil carbon. On the other hand, CIOA will have a majority of modern
703 carbon. In previous work we noted that 0 – 50% of the CIOA mass may be from non-cooking
704 sources and, specifically, from vehicles (Hayes et al., 2013). Furthermore, recent results have
705 shown that cooking emissions can form substantial amounts of SOA (El Haddad et al., 2012). If
706 P-S/IVOCs emitted with HOA are 100% fossil carbon, P-S/IVOCs emitted with CIOA are
707 25(±25)% fossil, and both emission sources form SI-SOA with the same efficiency, then the
708 corresponding amount of fossil urban SOA in the model would be 65(±9)%, 63(±12)%,
709 62(±12)%, and 78(±7)% for ROB+TSI, GRI+TSI, PYE+TSI, and ROB+4xV, respectively. It
710 should be noted that these percentages do not include BG-SOA because the ¹⁴C results from
711 Zotter et al. (2014) correspond to SV-OOA. None of these predictions are significantly different
712 from the ¹⁴C measurements. An important caveat is that P-S/IVOCs from CIOA-cooking sources
713 are modeled using the same parameters as P-S/IVOCs from HOA-vehicle sources. It is possible
714 that cooking and vehicle emissions do not exhibit the same SOA-forming properties, but it is not
715 clear which would be a more potent SOA precursor as there are no parameterizations specific to
716 cooking emissions available in the literature. Thus, the ROB, GRI, and PYE parameterizations
717 are used for all P-S/IVOCs regardless of their source, and the amount of SOA from HOA (or
718 CIOA) associated P-S/IVOCs can be calculated as simply the product of the total SI-SOA and
719 the ratio HOA/POA (or CIOA/POA), where the hourly HOA, CIOA, and SI-SOA concentrations
720 are used. It should also be noted that in Los Angeles gasoline contains nearly 10% ethanol made
721 from corn and thus modern carbon (de Gouw et al., 2012), but it is thought that ethanol and its
722 combustion products are not incorporated into aerosols (Lewis et al., 2006).

723 It should be noted that the fossil/modern split from the box model that is described above
724 depends on the initial P-S/IVOCs concentrations and volatility distribution assumed in the
725 model. These parameters are not well constrained for cooking emissions, as discussed in further
726 detail in Section 3.1.4 below. In addition, as discussed in the previous section (3.1.1) the
727 concentration of primary IVOCs in the box model is higher than that measured. Thus, As an
728 extreme sensitivity study, the model variations were also run under the assumption that CIOA

729 | [cooking](#) sources did not emit any P-S/IVOCs or, in the case of the PYE+TSI variation, any
730 SVOCs (Figure SI-5). [In this sensitivity study there is improved model/measurement agreement](#)
731 [for the primary IVOCs as shown in Table SI-3.](#) The GRI+TSI, PYE+TSI, and ROB+4xV
732 variations reasonably reproduce the SV-OOA concentrations with some periods outside the
733 measurement uncertainties. In contrast, the ROB+TSI variation without cooking-related P-
734 S/IVOCs predicts concentrations that are too low. Regardless of the parameterization, a strong
735 urban source of non-fossil SOA precursors, such as cooking emissions, must be included to
736 obtain agreement with the ¹⁴C measurements; otherwise the modeled SOA is overwhelmingly
737 fossil. Clearly, there are still large uncertainties in SOA formation from cooking emissions.
738 Further studies are needed to constrain models and to identify potential additional urban sources
739 of non-fossil SOA, although our results suggest that cooking emissions are a potentially
740 important source of anthropogenic non-fossil SOA.

741

742 **3.1.3. SOA concentration apportionment to precursor compounds**

743 The diurnal cycles of V-SOA mass concentration produced from individual VOCs are
744 shown in Figure 5A. Among the VOCs the five largest contributors to V-SOA are methyl-
745 substituted aromatics such as xylenes, trimethylbenzenes, and toluene. When SOA
746 concentrations peak, these compounds account for ~70% of the predicted V-SOA mass. In
747 Figure 5B the precursor-specific model predictions are compared against results from a
748 methodology developed by the U.S. EPA that apportions SOA to specific precursors using
749 molecular tracers measured in ambient aerosol samples (Kleindienst et al., 2012). For
750 methylbenzenes (i.e. aromatics containing one or more methyl substituents) the tracer molecule
751 utilized is 2,3-dihydroxy-4-oxopentanoic acid, and for naphthalene, 1-methylnaphthalene, and 2-
752 methylnaphthalene the tracer molecule is phthalic acid and its associated methyl-containing
753 analogs. Several tracers are used for isoprene (Edney et al., 2005) and monoterpenes (Jaoui et al.,
754 | 2005; Claeys et al., 2007; Szmigielski et al., 2007), and they are listed in Table SI-~~43~~
755 supporting information.

756 For the methylbenzenes, the model/tracer comparison is good, indicating consistency
757 between model predictions and ambient measurements. The similarity further validates the
758 model, although it is noted that if V-SOA ‘aging’ is eliminated from the model the model/tracer

759 comparison improves further and the difference becomes less than 5%. We note that this
760 comparison cannot constrain whether chamber yields have been reduced by vapor losses, since
761 the same effect would have occurred when measuring the yields included in the model and when
762 measuring the SOA/tracer ratio used for the tracer estimate.

763 For the biogenic VOCs, isoprene and the monoterpenes, the tracer estimate indicates
764 several-fold higher concentrations than predicted in the model. This difference is not surprising
765 since the background SOA is thought to have a major contribution from isoprene and
766 monoterpene oxidation in areas north of the Los Angeles Basin, and in the model BG-SOA from
767 different VOCs is not resolved. In other words, the model results in Figure 5B represent only the
768 in-basin biogenic SOA and are lower limits for total SOA from isoprene and monoterpenes.
769 Moreover, the tracer estimates in Figure 5B are likely lower limits as well because the tracers
770 may be lost by subsequent physical or chemical processes occurring in very aged aerosol
771 transported to the measurement location (Hallquist et al., 2009). If the tracer molecule is
772 oxidized or oligomerized, then it will be effectively lost with respect to the tracer method, even if
773 its mass stays in the particle phase. If a semi-volatile tracer evaporates during atmospheric
774 transport or from the filter after sampling, it is also lost from the point of view of the tracer
775 method even though a chemical reaction has not occurred. It appears that the
776 model/measurement comparison for the biogenic VOCs is qualitatively consistent given the
777 known limitations of both approaches. However, the amount of SOA from biogenic VOCs as
778 determined by the tracer method is only ~10% of the BG-SOA (0.22 versus 2.1 $\mu\text{g m}^{-3}$) even
779 though the BG-SOA is predominantly biogenic as previously noted. The most likely explanation
780 for the difference in mass concentration is the loss mechanisms described above. Other possible
781 sources for the background such as biomass burning or marine OA are known to be very low at
782 this location (Hayes et al., 2013), and more than 69% of the LV-OOA stems from non-fossil
783 sources (Zotter et al., 2014).

784 Figure 5B also shows a comparison for the naphthalenes. The tracer estimates are over an
785 order-of-magnitude higher than the model predictions when using the SOA yields from the
786 literature (which are ~20% for the conditions of our study) and the emission ratios determined
787 from the regression analysis of nighttime measurements shown in Figure SI-3. The model is also
788 run using the empirically adjusted emission ratios that better match the observed concentrations

789 | of the naphthalenes. ~~One can observe that~~ The model for this variation is still much lower than
790 | the tracer estimate. As an additional sensitivity study, we also run the model with the adjusted
791 | emissions and a yield of 150% that places all the oxidized mass in the $C^*=1 \mu\text{g m}^{-3}$ volatility bin.
792 | This last variation represents an upper limit estimate of SOA from naphthalenes, in which nearly
793 | all of the mass plus the added oxygen partitions to the particle phase, which is much higher than
794 | laboratory observations. The tracer estimate, however, is still about a factor of two higher than
795 | the model. It is known that the tracer estimate is an upper limit, because the tracer compound,
796 | phthalic acid, may not be a unique tracer, and it potentially could be emitted from primary
797 | sources (Kleindienst et al., 2012). ~~However, there may be other alkylated or functionalized PAHs~~
798 | ~~that are not explicitly accounted for in the box model, and some of them might produce this~~
799 | ~~tracer. Thus, when considering this limitation it is concluded the model/measurement~~
800 | ~~comparison is consistent.~~

801 | The best estimate from the model with the adjusted emissions results in 0.7% of the
802 | predicted SOA being formed from the measured naphthalenes. Utilizing the upper limit of the
803 | model results for ~~the PAHs~~naphthalene, including that from the parameterization with a
804 | purposefully high yield, it is apparent that naphthalene, 1-methyl naphthalene, and 2-methyl
805 | naphthalene and its analogs account for less than 4% of the SOA mass. While previous work has
806 | suggested that PAHs are important precursors for SOA in the Los Angeles BasinSøCAB (Hersey
807 | et al., 2011) these earlier findings were qualitative and based on the observation of phthalic acid
808 | in samples. The work presented here, ~~both the modeling results as well as the tracer results,~~
809 | quantitatively demonstrates that SOA from identified naphthalene, 1-methylnaphthalene, and 2-
810 | methylnaphthalene PAHs is relatively ~~unimportant~~ small but not negligible when compared to
811 | ~~other precursors such as methylbenzene~~ the total SOA concentration. An upper limit for the
812 | contribution of, with this group of precursors accounting for at most is 8(±3)% of the SOA. (This
813 | percentage is calculated using the tracer method in which the SOA concentration from PAHs is
814 | higher than in the box model and a 30% uncertainty for the SV-OOA concentration.) Lastly, we
815 | note that no suitable tracers for alkane oxidation have been identified yet, which prevents
816 | carrying out similar model/tracer comparisons with respect to the P-S/IVOCs, ~~which~~since these
817 | compounds are thought to be composed primarily, although not exclusively, of alkanes.

818

819 **3.1.4. SOA concentration apportionment to gasoline vehicles, diesel vehicles,**
820 **cooking activities, and in-basin biogenic sources**

821 In addition to apportioning the amount of SOA formed from individual compounds there
822 is also considerable recent interest in the apportionment of SOA between diesel and gasoline
823 vehicle emissions as well as other urban sources (Bahreini et al., 2012; Gentner et al., 2012;
824 Hayes et al., 2013; Ensberg et al., 2014). The SOA model developed here can be used to address
825 this important problem, and in Figure 6 the urban SOA mass calculated in the model is
826 apportioned between diesel vehicles, gasoline vehicles, cooking sources, and in-basin biogenic
827 emissions. The SOA mass is apportioned to each source using the following method, which can
828 be described in five steps. First, the background is set to $2.1 \mu\text{g m}^{-3}$. Second, the in-basin
829 biogenic SOA is calculated as described in the methods section. Third, for the diesel
830 contribution, since it is estimated that $70(\pm 10)\%$ of HOA is emitted from diesel vehicles (Hayes
831 et al., 2013), it is assumed in the model that 70% of the P-S/IVOCs co-emitted with HOA are
832 from diesel vehicles as well. (The remainder is assumed to be from gasoline vehicles.) While
833 VOCs emissions from diesel vehicles are low (Warneke et al., 2012) in the Los Angeles Basin,
834 VOCs have still been measured in diesel fuel. Specifically, using the measurements of Gentner et
835 al. (2012) given in Tables S9 and S10 of that paper, the percentage of each VOC included in our
836 model emitted from diesel vehicles is calculated. The precursor-specific SOA concentrations, as
837 shown in here in Figure 5, are then multiplied by these percentages to determine the fraction of
838 V-SOA attributable to diesel emissions, which is 3%. It should be noted that for all the VOCs
839 included here except 1,3-butadiene, styrene, and anthropogenic isoprene, the corresponding
840 concentrations in gasoline and diesel fuel are published in Gentner et al. (2012). Fourth, the
841 cooking contribution is calculated by assuming that 75% of the P-S/IVOCs co-emitted with
842 CIOA are from cooking activities. This percentage is chosen since it lies halfway between 50 and
843 100%, which is the current constraint from measurements on the amount of CIOA from cooking
844 sources as discussed above and in Hayes et al. (2013). Fifth, the gasoline fraction is taken to be
845 the SOA formed from all the remaining VOCs as well as the remaining P-S/IVOCs.

846 As can be seen in Figure 6, for the urban SOA (i.e. excluding the background OA) diesel,
847 gasoline, and cooking emissions all contribute substantially to SOA formation, with the sum of
848 gasoline and cooking being much larger than diesel for all model variants. In contrast, the in-

849 basin biogenic contribution is small. The analogous results when the background is included are
850 shown in the supporting information (Figure SI-6). The formation of SOA from diesel emissions
851 accounts for 16 – 27% of the urban SOA in the model depending on the variant used. This result
852 is very similar to the percentage reported in our previous work, 19(+17/-21)%, which was
853 determined using measurements of OOA weekly cycles (Hayes et al., 2013). In addition, the
854 existence of a diesel contribution in the model is consistent with PMF analysis of FTIR spectra
855 of OA filter samples collected in Pasadena, in which, one SOA component exhibited relative
856 peak intensities in the C-H stretching region that suggest some qualitatively a contribution from
857 diesel emissions (Guzman-Morales et al., 2014). although the percentage of SOA from diesel
858 could not be determined in this previous work. The results of our work stand in contrast to those
859 of Gentner et al. (2012) however, wherein the contribution of diesel and gasoline to vehicular
860 SOA were estimated to be 70% and 30%, respectively. This discrepancy may be due to the
861 assumption used by Gentner et al. that effectively all vehicle emissions are unburned fuel,
862 whereas recent experiments have indicated that important SOA precursors exist in gasoline
863 vehicle emissions that are not present in unburned gasoline when after-treatment devices such as
864 catalytic converters are used (Jathar et al., 2013).

865 Also shown in Figure 6 is a bar graph summarizing the result from each parameterization
866 grouped by fossil and non-fossil sources as well as the fossil fraction of SV-OOA determined by
867 Zotter et al. (2014). The results of the two studies are consistent, with cooking and in-basin
868 biogenic SOA accounting for between 23 – 38% of the in-basin SOA mass in the models. These
869 two sources represent the modern fraction in the box model.

870 The uncertainties shown in Figure 6 (in parentheses) are calculated by propagating the
871 uncertainty in the amount of HOA from diesel sources, as well as the uncertainty in the amount
872 of CIOA from cooking sources under the assumption that the P-S/IVOCs co-emitted with these
873 primary aerosols have similar uncertainties. It is also noted that another source of uncertainty is
874 the selection of the ROB+TSI, GRI+TSI, PYE+TSI, or ROB+4xV model variation. The model
875 variant used has an important impact on the apportionment, but the greatest amount of urban
876 SOA formed from diesel emissions when considering all the uncertainties described in this
877 paragraph is still only 31%.

878 The uncertainties in Figure 6 do not however account for certain assumptions that were
879 made in order to perform the source apportionment. In particular, it was assumed that the P-
880 S/IVOCs to POA ratio as well as the volatility distribution of P-S/IVOCs is the same for all
881 sources, which is likely not the case. However, to our knowledge there is insufficient information
882 in the literature to prescribe different volatility distributions for different sources.

883 Lastly, the percentage of SOA attributed to cooking emission in this work also requires
884 discussion. Compared to gasoline or diesel vehicles there is relatively little data on the SOA
885 forming potential of cooking emissions, but nevertheless there is both direct and indirect data
886 supporting the SOA forming potential of cooking emissions. First, it is clear from numerous
887 source apportionment studies that cooking emissions are a source of organic matter in the
888 atmosphere (e.g. Robinson et al., 2006; Mohr et al., 2011; Hayes et al., 2013). Second, molecular
889 speciation of cooking emissions has demonstrated that cooking activities emit a variety of
890 volatile and semi-volatile compounds that are known SOA precursors (Schauer et al., 1999,
891 2002). Third, chamber studies have demonstrated SOA formation from cooking emissions. The
892 latter results have been presented at several major conferences, but have not yet been published
893 in the peer-reviewed literature (El Haddad et al., 2012). Thus, it is reasonable to conclude that
894 SOA models should include the SOA resulting from chemical processing of cooking emissions,
895 but there is a lack of chamber yields that could be used to develop specific SOA
896 parameterizations. We have therefore assumed that SOA from cooking emission can be
897 described using the same parameterizations as used for SOA from vehicular P-S/IVOCs. We
898 have also performed a sensitivity study where we assume that cooking emissions do not produce
899 any SOA. Ultimately, the percentage of SOA from cooking emissions reported here should be
900 considered a first-order estimate that should be updated when additional data regarding SOA
901 from cooking emissions becomes available.

902

903 **3.1.5. Evolution of SOA concentration for 3 days**

904 It is of high interest to explore the evolution of the different parameterizations discussed
905 here at greater photochemical ages than those observed at the Pasadena site, since this behavior
906 can lead to different results in regional and global modeling studies, and since similar
907 combinations of parameterizations were found to overpredict regional SOA downwind of

908 Mexico City (Dzepina et al., 2011). To explore this question, the evolution of SOA concentration
909 was simulated for 3 days using each of the four major variations (ROB+TSI, GRI+TSI,
910 PYE+TSI, ROB+4xV). The same simulation was carried out for the SIMPLE model and it is
911 discussed below in Section 3.3. The results are shown in Figure 7, and in order to facilitate
912 comparisons the SOA concentrations are normalized to the CO concentration, after subtracting
913 the CO background (DeCarlo et al., 2010). These simulations are for continuous aging at a
914 reference •OH concentration of 1.5×10^6 molec cm^{-3} , and thus, they do not attempt to simulate a
915 diurnal variation in the amount of photochemical aging. This approach is used because it
916 facilitates the comparison against field measurements described below. Furthermore, the box
917 model does not account for how dilution downwind of Los Angeles may increase SOA
918 evaporation and thus the rate of oxidation via increased partitioning to the gas phase. However,
919 this phenomenon would only lead to small changes in total model SOA, and that should not
920 change the conclusions discussed in this section (Dzepina et al., 2011). Also shown in Figure 7 is
921 the same ratio, $\text{SOA}/\Delta\text{CO}$, determined previously from measurements at the Pasadena site
922 (Hayes et al., 2013). At photochemical ages less than 0.25 days, GRI+TSI and ROB+4xV
923 perform the best (Table 4), which is consistent with the comparisons against the diurnal average
924 of SOA since the diurnal photochemical age peaks at about 0.25 days (Figure 3A). However, for
925 higher photochemical ages between 0.25 and 0.5 days the performance of ROB+TSI improves.

926 | We also note that all of the parameterizations used in this section produce $\text{SOA}/\Delta\text{CO}$
927 ratios substantially larger (by factors of 2 or more) than those observed globally for aged air
928 masses (i.e. photochemical ages greater than one day at an average OH concentration of 1.5×10^6
929 molec cm^{-3}). For reference the range of $\text{OA}/\Delta\text{CO}$ ratios reported by de Gouw and Jimenez
930 (2009) for aged urban SOA across multiple sites is indicated by the gray regions in Figure 7.
931 This $\text{OA}/\Delta\text{CO}$ ratio includes both POA and SOA, but POA is a small contributor to $\text{OA}/\Delta\text{CO}$ for
932 very aged air. Also shown in Figure 7 is the $\text{SOA}/\Delta\text{CO}$ ratio observed by Bahreini et al. (2012)
933 from the NOAA P3 aircraft in the Los Angeles Basin outflow where air masses were aged from
934 1 – 2 days. This ratio is similar to the range taken from de Gouw and Jimenez (2009). The
935 differences between the modeled and the measured $\text{SOA}/\Delta\text{CO}$ at higher photochemical ages may
936 be important for regional and global models as they suggest an overestimation of urban SOA
937 downwind of polluted regions. One possible explanation for the higher predicted values is the
938 lack of a fragmentation mechanism in the parameterizations, which would reduce the SOA mass

939 by producing higher volatility products. Indeed, decreases in SOA concentration at high
940 photochemical ages have been observed in flow-tube studies, although typically at
941 photochemical ages much longer than 3 days (George and Abbatt, 2010). Also dry deposition in
942 the regional models may decrease over-prediction depending on how it is implemented (Knote et
943 al., 2014a).

944 A third explanation is the potential overestimation of IVOC emissions in the box model.
945 As discussed in Section 3.1.1, the initial concentration of primary IVOCs in the model is a factor
946 of 2 higher than the values determined from field measurements by Zhao et al (2014). To
947 investigate this possibility, a sensitivity study was run in which the initial concentrations of
948 primary IVOCs in the volatility bins $C^* = 10^3, 10^4, 10^5,$ and 10^6 were decreased by one-half. The
949 results of this sensitivity study are shown in Figure 8. In general, ROB+TSI, GRI+TSI,
950 PYE+TSI and ROB+4xV all show better agreement with measurements at long photochemical
951 ages, although all four variants still overestimate the measurements. For shorter photochemical
952 ages (in the urban scale) ROB+TSI under-predicts the SOA concentration, whereas GRI+TSI
953 and ROB+4xV both predict SOA/ Δ CO ratios that are not significantly different from the
954 measured values (Hayes et al., 2013), and lastly PYE+TSI overestimates the SOA concentration.
955 Thus, IVOCs emissions that are too high in the box model may be responsible for some, but not
956 all, of the overestimation of SOA concentrations at long photochemical ages.

957 For reference, we note that when the IVOC concentrations are halved the four variations
958 all predict less SI-SOA for the Pasadena ground site (Figure SI-7), but the contribution of P-
959 S/IVOCs to SOA formation remains important: 59 – 73% (ROB+TSI), 72 – 80% (GRI+TSI), 79
960 – 92% (PYE+TSI), 38 – 48% (ROB+4xV). Furthermore, all four variations still predict a fossil
961 fraction of urban SOA consistent with the ^{14}C measurements at the Pasadena site: 66(\pm 9)%,
962 64(\pm 10)%, 61(\pm 12)%, 78(\pm 6)%, respectively. Note that in calculating these fossil fractions the
963 IVOCs emissions from cooking and gasoline/diesel were reduced by the same amount (i.e. one-
964 half).

965

966 **3.1.6. Comparison of WRF-CMAQ versus measurements and box model**

967 The comparison of the SOA predicted for Pasadena by the WRF-CMAQ model is shown
968 in Figure 89A. Unlike the box model, the 3-D WRF-CMAQ model simulates the production and

969 transport of SOA both within and outside the Los Angeles Basin. It is therefore most appropriate
970 to compare the WRF-CMAQ model output with OOA (SV-OOA + LV-OOA) rather than just
971 SV-OOA as is done for the box model that focused only on the urban area. The WRF-CMAQ
972 SOA is well correlated with the measured OOA ($R= 0.73$), but the SOA mass concentration in
973 the model is ~25 times lower than the observed amount. This discrepancy is observed despite the
974 fact that the VOCs show reasonable agreement (Supporting Information Figure SI-87, Panels A –
975 C). The difference of a factor of 25 in the SOA concentrations is also observed consistently
976 across different photochemical ages (Supporting Information Figure SI-87, Panel D).
977 Furthermore, the performance of WRF-CMAQ is good for the inorganic aerosol species
978 (Supporting Information Figures SI-98 and SI-109) as well as for elemental carbon and different
979 meteorological parameters (Baker et al., 2013; Kelly et al., 2014). These comparisons indicate
980 that while the model appears to be accurately simulating the transport to Pasadena and
981 photochemical aging, the amount of SOA formed from urban precursors is greatly
982 underestimated by WRF-CMAQ. Given the importance of P-S/IVOCs as SOA precursors in the
983 box model, the lack of these species in WRF-CMAQ explains a substantial fraction of the
984 difference between the models.

985 To further examine both WRF-CMAQ and the box model results, we modify the SOA
986 module of the box model to be similar to the treatment of urban SOA in WRF-CMAQ as
987 described by Carlton et al. (2010). First, for the box model P-S/IVOCs are not included, since
988 these species are not in WRF-CMAQ. Second, the BG-SOA in the box model is adjusted to 0.1
989 $\mu\text{g m}^{-3}$ so that the concentrations of SOA in the two models are similar in the early morning
990 hours when the background dominates. Third, the box model uses a different approach for
991 simulating V-SOA identical to that described by Dzepina et al. (2009). Briefly, instead of the
992 VBS, an empirical 2-product parameterization wherein the oxidized products cannot undergo
993 aging is used (Koo et al., 2003).

994



996

997 The effective saturation concentration for each lumped product, *SVOC*, is then used to calculate
998 the equilibrium partitioning between gas- and particle-phases as shown earlier in Equation 1.

999 | Also, in Equation 3, α is the yield for each VOC. Note that the Koo et al. (2003)
1000 | parameterization produces substantially lower V-SOA yields than the Tsimpidi et al. (2010)
1001 | parameterization used in the rest of this work. The latter parameterization was updated using
1002 | more recent chamber results (with higher yields) such as those of Ng et al. (2007). The use of the
1003 | older Koo et al. (2003) parameterization for this specific comparison was motivated by the fact
1004 | that the parameterization for urban SOA in the version of CMAQ used here is based on the same
1005 | older data and does not contain the higher updated yields in, for example, Tsimpidi et al. (2010).

1006 | The results of the comparison of WRF-CMAQ with the modified box model are shown in
1007 | Figure 89B. With those modifications the results are very similar. This good agreement indicates
1008 | that the differences between the default box model and WRF-CMAQ are not due to differences
1009 | in transport or another variable, but rather the intrinsic differences in the SOA modules. In
1010 | addition, the comparison between the two models suggests that 3-D air quality models need to
1011 | include either SOA from P-S/IVOCs, additional precursor sources, and/or increased V-SOA
1012 | yields to accurately predict SOA concentrations in the Los Angeles Basin and other urban areas.

1013 |

1014 | **3.2. Comparison of predicted and measured SOA oxygen content**

1015 | The diurnal cycle of O:C of total OA is shown in Figure 910, along with the estimated
1016 | $\pm 30\%$ uncertainty of the O:C determination (Aiken et al., 2007; 2008). A recent re-evaluation of
1017 | the AMS elemental analysis has found an underestimation of oxygen content for multi-functional
1018 | oxidized organics (Canagaratna et al., 2015). Thus, the updated calibration factors have been
1019 | used in the work here, and they increase the measured O:C and H:C by factors of 1.28 and 1.1,
1020 | respectively. The model predictions of O:C are shown for both the ROB+TSI and GRI+TSI
1021 | variations. The measured O:C is similar or higher than the models, and exhibits only small
1022 | changes during the day. The minimum after noon in the measured O:C is due to the arrival of
1023 | POA above Pasadena as well as the production of fresh SOA. The second minimum in the
1024 | evening is due to emissions of CIOA, which has relatively low oxygen content.

1025 | When the model is run with the ROB+TSI variation for O:C evolution in SOA the model
1026 | diurnal cycle is generally lower than the field data. Similar to the comparison of mass
1027 | concentration, the GRI+TSI model variation better reproduces the O:C observations. As a control
1028 | the model is also run without SI-SOA, which, interestingly, also does an excellent job of

1029 reproducing the observations. Two conclusions can be drawn from the results shown in Figure
1030 [910](#). First, the SI-SOA in the ROB parameterization appears to be not sufficiently oxidized,
1031 which drives down the predicted O:C, and, in general, SOA production and oxidation in
1032 Pasadena is very rapid and is therefore best described by the GRI parameterization. Second, both
1033 SI-SOA from the GRI parameterization and V-SOA have an O:C of ~ 0.45 , which is not very
1034 different from the weighted mean of HOA, CIOA, and LV-OOA (O:C ~ 0.6), and, as a result, the
1035 total OA O:C is relatively constant for the different times of day. This consideration also
1036 explains why O:C does not change substantially when the SI-SOA is included or excluded in the
1037 model.

1038 Lastly, we note that there are large uncertainties in the parameters used to predict O:C
1039 such as the distribution of O:C values as a function of volatility for V-SOA or the amount of
1040 oxygen mass added to the SI-SOA for each oxidation reaction. It is therefore not very
1041 meaningful to conclude from this study that one parameterization performs better than another.
1042 Rather, it is apparent that when using several different previously published SOA
1043 parameterizations (i.e. ROB+TSI, GRI+TSI, and TSI alone) it is possible to reproduce the
1044 observed O:C at the Pasadena ground site.

1045

1046 **3.3. A simple parameterization for SOA formation in polluted urban regions**

1047 While medium-complexity parameterizations of SOA formation and evolution such as
1048 those used above represent some important details of SOA chemistry and properties, there is a
1049 need for very computationally inexpensive SOA parameterizations that still retain good accuracy
1050 for use in regional, global, and climate models. Such a parameterization was recently reported by
1051 Hodzic and Jimenez (2011), and was designed to predict properties of urban SOA in global and
1052 climate modeling studies (referred to as the “SIMPLE” parameterization hereinafter). The model
1053 represents SOA precursors as a single surrogate lumped species, termed here ‘VOC*’, which is
1054 emitted proportionally to anthropogenic CO. The model converts VOC* to SOA by reaction with
1055 $\bullet\text{OH}$ with a specified rate constant. The SOA formed in the SIMPLE model is non-volatile and
1056 does not partition to the gas-phase, consistent with the low volatility observed for aged SOA in
1057 field studies (e.g., Cappa and Jimenez, 2010).

1058 We replaced the SOA parameterizations discussed above with the SIMPLE
1059 parameterization just described, and ran the box model for a large number of possible parameter
1060 value combinations (i.e. emission ratio of VOC*/CO and •OH rate constant). Figure 110A shows
1061 the difference between model and measurement over that parameter space. The diurnal cycle
1062 predicted by the SIMPLE parameterization with the optimum parameters for Pasadena is shown
1063 in Figure 110B. The SIMPLE model with the optimized parameters performs comparably to the
1064 more complex parameterizations used in this work. At the same time, the SIMPLE
1065 parameterization is unable to capture perfectly the location of the peak in time because it
1066 depends solely on CO and photochemical age. The CO concentration at the site peaks at 12:00
1067 and photochemical age peaks at 13:00 (Figure 3A) while the measured SOA has a broad peak
1068 between 14:00 – 16:00. The fact that SOA does not peak at the same time as CO and
1069 photochemical age indicates the assumption in SIMPLE that VOC*/CO does not vary in time is
1070 probably not completely accurate. Still, the performance of the SIMPLE parameterization for
1071 urban SOA is sufficient for many applications and certainly far better than many models
1072 currently used.

1073 Interestingly, the optimal model parameters for Mexico City and Pasadena are very
1074 similar. In other words, when tuning the model separately for each city, the parameters obtained
1075 are identical within the estimated uncertainties. -which This result suggests ~~the SIMPLE model,~~
1076 with the parameters reported for Mexico City or Pasadena, can be applied to other polluted urban
1077 regions as well. In addition, the optimal parameters for Pasadena (and Mexico City) are
1078 consistent with the OA/ Δ CO ratios observed for highly aged air masses by Bahreini et al. (2012)
1079 from the NOAA P3 aircraft in the LA basin outflow, as well as for other urban areas as
1080 summarized by de Gouw and Jimenez (2009) and shown in Figure 7. However, it should be
1081 noted that a range of SIMPLE parameter combinations still remains in which the different
1082 combinations perform similarly in the model/measurement comparison, and this range is
1083 indicated by the dashed box in Figure 110A. ~~This lack of a precise constraint is due to, in part,~~
1084 ~~the limited range of photochemical ages observed at most stationary field sites. Thus~~ While the
1085 SIMPLE model is promising, additional work should be carried out to verify the optimal
1086 SIMPLE model parameters including analysis of data for a broad range of ages, e.g., by utilizing
1087 results from ambient air processed by oxidation flow reactors (Ortega et al., 2013). Also, the
1088 accuracy of the SIMPLE model for predicting urban SOA under a variety of atmospheric

1089 | conditions should be explored (e.g. VOC/NO_x or relative amounts of gasoline versus diesel
1090 | emissions.) Finally, we note that the SIMPLE model parameterizes urban SOA, and is not
1091 | applicable to biogenic SOA.

1092 | Hodzic and Jimenez (2011) also proposed an approach for predicting the oxygen content
1093 | of SOA that utilized the equation $O:C = 1 - 0.6\exp(-A/1.5)$, where A is the photochemical age in
1094 | days. (Note: the photochemical age was calculated using a reference •OH concentration of
1095 | 1.5×10^6 molec cm⁻³.) As shown in Figure 124, this parameterization compares well with the O:C
1096 | from measurements. However, the parameterization of Hodzic and Jimenez does not take into
1097 | account the new AMS O:C calibrations factors, as described in the preceding section. In order to
1098 | account for this change, the equation proposed by Hodzic and Jimenez must be multiplied by a
1099 | factor of 1.28. Thus, the updated parameterization is $O:C = 1.28(1 - 0.6\exp(-A/1.5))$, and the
1100 | corresponding O:C values are shown in Figure 124. The updated simple parameterization also
1101 | exhibits good agreement with measurements. (Note: The O:C predicted by the updated model
1102 | does not increase by a factor 1.28 relative to the original version because the SOA from the
1103 | Hodzic and Jimenez parameterization is mixed with HOA, CIOA, and BG-SOA to determine the
1104 | total OA O:C shown in Figure 124.)

1105

1106 | **3.4 Update of the U.S. and Global Urban SOA budgets**

1107 | As shown in Figure 7, the SIMPLE parameterization asymptotically approaches a
1108 | SOA/ Δ CO value of $80 \mu\text{g m}^{-3} \text{ppm}^{-1}$, which can be used to estimate an urban SOA budget. The
1109 | SIMPLE parameterization is better for estimating this budget than the more complex
1110 | parameterizations, because the SIMPLE parameterization is consistent with the observations of
1111 | de Gouw and Jimenez (2009) that were made at multiple locations. For the ROB+TSI, GRI+TSI,
1112 | PYE+TSI, and ROB+4xV model variants, values of SOA/ Δ CO between 150 and $220 \mu\text{g m}^{-3}$
1113 | ppm^{-1} are predicted at long photochemical ages, and such high values have never been observed,
1114 | to our knowledge, downwind of anthropogenic-dominated sources. These four more complex
1115 | parameterizations are based on laboratory data at short photochemical ages, and thus, applying
1116 | them to long photochemical ages is an extrapolation. The SIMPLE parameterization is imperfect,
1117 | but based on the available evidence it appears that the SIMPLE model is the most accurate at
1118 | long photochemical ages and better suited for estimating the urban SOA budget.

1119 For the U.S., the annual urban CO emissions reported in the 2011 NEI are 44 Tg yr⁻¹
1120 (EPA, 2013), which when multiplied by SOA/ Δ CO gives an national urban SOA source of 3.1
1121 Tg yr⁻¹. ~~For reference, from the same database the national biogenic VOCs emissions are 37 Tg~~
1122 ~~yr⁻¹. Then using an approximate yield of 10%, the biogenic VOCs would represent a SOA source~~
1123 ~~of 3.7 Tg yr⁻¹. While there are several major uncertainties in this analysis—the accuracy of the~~
1124 ~~SIMPLE model at greater photochemical ages, yields for biogenic VOCs, etc.—it is evident that~~
1125 ~~the amount of urban SOA is not negligible compared to the amount of biogenic SOA in the U.S.~~
1126 The same estimate can be performed for global urban SOA, since similar ratios of SOA/ Δ CO
1127 have been observed in other countries such as downwind of Mexico City and China (DeCarlo et
1128 al., 2010; Hu et al., 2013). Using the EDGAR v4.2 inventory of 371 Tg yr⁻¹ of urban/industrial
1129 CO for 2008 (JRC, 2011), we estimate a global pollution SOA source of 26 Tg yr⁻¹, or about
1130 17% of the estimated global SOA source of 150 Tg yr⁻¹ (Hallquist et al., 2009; Heald et al., 2010;
1131 Heald et al., 2011; Spracklen et al., 2011). We note that 1/3 of that SOA would be non-fossil, if a
1132 similar cooking fraction is observed globally as in this study, which is expected given the
1133 identification of similar fractions of cooking POA in many field studies globally (Wang et al.,
1134 2009; Mohr et al., 2011; Sun et al., 2011).

1135

1136 4. Conclusions

1137 SOA in Pasadena during CalNex has been modeled using three different methods: (1) a
1138 box model, (2) a 3-D dimensional al model, namely, WRF-CMAQ, and (3) a simple two-parameter
1139 model. Model/measurement comparisons clearly indicate that SOA formed from P-S/IVOCs, or
1140 a similar source, must be included in the models to accurately predict SOA concentrations in
1141 Pasadena. In other words, SOA from VOC oxidation is not sufficient to explain the observed
1142 concentrations, even when the highest SOA yields are used. Specifically, the parameterizations
1143 utilized were the Tsimpidi et al. (2010) parameterization with aging or a modified version of that
1144 parameterization in which the SOA yields for aromatic VOCs were multiplied by four as recently
1145 suggested by Zhang et al. (2014).

1146 Three parameterizations for SOA formation from P-S/IVOCs were tested. It was found
1147 that the parameterization reported by Grieshop et al. (2009) best predicts ~~both~~ SOA
1148 concentration at the urban site ~~and SOA oxygen content~~. In contrast, the parameterization of

1149 | Robinson et al. (2007) predicts too little SOA ~~and too low oxygen content~~. These results contrast
1150 | earlier modeling studies of Mexico City that showed the Robinson parameterization performed
1151 | better when compared against the measured SOA concentration. The reason for the difference is
1152 | not clear ~~a different mixture of P-S/IVOCs at the two locations~~. Both the Mexico City and
1153 | Pasadena studies suggest indicate that the Grieshop parameterization more accurately predicts
1154 | SOA oxygen content, but this conclusion is also dependent on model parameters that are not
1155 | well-constrained. Additionally, we tested the parameterization proposed in Pye and Seinfeld
1156 | (2010) for the formation of SOA from P-S/IVOCs, which produces similar results but tends to
1157 | overpredict SOA concentrations especially at nighttime and in the morning for this case study.
1158 | The relative importance of VOCs and P-S/IVOCs as contributors to urban SOA over different
1159 | time and length scales remains unclear. Depending on the parameterization used in the box
1160 | model, the amount of urban SOA from VOCs can range between 15 – 53% of the total predicted
1161 | SOA for the Pasadena ground site. This range is 16 – 58% in a sensitivity study in which the
1162 | IVOC emissions are reduced by one-half. All the parameterizations used in the box model
1163 | overpredict urban SOA at photochemical ages larger than one day compared to field
1164 | observations, which has implications for their use in regional and global models. However, when
1165 | the IVOC emissions in the box model are reduced by one-half to better match the measurements
1166 | of Zhao et al. (2014) the predictions of SOA at long photochemical are improved although still
1167 | too high, while the model/measurement comparison at short photochemical ages is still within
1168 | the measurement uncertainties for the GRI+TSI and ROB+4xV variations.

1169 | This work represents the first chemically explicit evaluation of WRF-CMAQ SOA mass
1170 | predictions in the Western U.S. or California. This model provides excellent predictions of
1171 | secondary inorganic particle species but underestimates the observed SOA mass by a factor of
1172 | about 25. The discrepancy is likely attributable to the VOC-only parameterization used that has
1173 | relatively low yields and does not include SOA from P-S/IVOCs or a similar source.

1174 | SOA source apportionment was also carried out using the box model results. Among the
1175 | explicitly modeled VOCs, the precursor compounds that contribute the most SOA mass are all
1176 | methylbenzenes. In contrast, measured PAHs (i.e. including naphthalene, 1-methylnaphthalene,
1177 | and 2-methylnaphthalene) are relatively minor precursors and contribute 0.7% of the SOA mass.
1178 | In addition, the amount of urban SOA from diesel vehicles, gasoline vehicles, and cooking-
1179 | related emissions is estimated to be 16 – 27%, 35 – 61%, and 19 – 35%, respectively, with an

1180 | almost factor of 2 difference in the estimated contribution depending on the box model variant
1181 | used. A significant amount of background SOA appears to be formed outside the Los Angeles
1182 | Basin and transported to the Pasadena site. The percentage estimated from diesel in the model is
1183 | in agreement with our previous study that estimated the diesel contribution to be 0 – 36% by
1184 | analyzing the weekly cycle of OOA concentrations (Hayes et al., 2013). The fraction of fossil
1185 | and non-fossil urban SOA from the different models is generally consistent with the
1186 | measurements. Importantly, a large source of urban non-fossil SOA most likely due to cooking is
1187 | identified, while biogenic SOA formed from urban-scale emissions makes a small contribution.

1188 | The final portion of this work adapts the SIMPLE two parameter model of Hodzic and
1189 | Jimenez (2011) to predict SOA properties for Pasadena. The simple model successfully predicts
1190 | SOA concentration and oxygen content with accuracy similar to the more complex
1191 | parameterizations. Furthermore, the optimal parameters for the SIMPLE model are very similar
1192 | in both Mexico City and Pasadena, which indicates that this computationally inexpensive
1193 | approach may be useful for predicting pollution SOA in global and climate models. Pollution
1194 | SOA is estimated to account for 17% of global SOA, and we note that ~1/3 of urban SOA may
1195 | be non-fossil mainly due to the impact of cooking and other sources.

1196

1197 | **Acknowledgements**

1198 | This work was partially supported by CARB 08-319 and CARB 11-305, US DOE (BER,
1199 | ASR program) DE-SC0006035, DE-SC0006711, and DE-SC0011105, NSF AGS-1243354 and
1200 | AGS-1360834, and NOAA NA13OAR4310063. PLH is also grateful for a fellowship from the
1201 | CIRES Visiting Fellows Program as well as and PLH and PKM acknowledge support from a
1202 | NSERC Discovery Grant and the Université de Montréal. The authors thank Chris J. Hennigan
1203 | (UMBC) and Allen L. Robinson (CMU) for providing the naphthalene and methylnaphthalene
1204 | data. We also thank John S. Holloway (NOAA) for providing CO data, Roya Bahreini
1205 | (University of California-Riverside) and Ann M. Middlebrook (NOAA) for providing OA data
1206 | from the NOAA P3, as well as Stuart A. McKeen (NOAA) for helpful discussions. RA is
1207 | supported by the US Weather Research Program within NOAA/OAR Office of Weather and Air
1208 | Quality. The US Environmental Protection Agency through its Office of Research and
1209 | Development collaborated in the research described here. The manuscript is being subjected to

1210 external peer review and has not been cleared for publication. Mention of trade names or
1211 commercial products does not constitute endorsement or recommendation for use.

1212 **References**

1213

- 1214 Ahmadov, R., McKeen, S.A., Robinson, A.L., Bahreini, R., Middlebrook, A.M., de Gouw, J.A.,
 1215 Meagher, J., Hsie, E.Y., Edgerton, E., Shaw, S. and Trainer, M. (2012) A volatility basis
 1216 set model for summertime secondary organic aerosols over the eastern United States in
 1217 2006. *J. Geophys. Res.-Atmos.* 117, D06301.
- 1218 Aiken, A.C., DeCarlo, P.F. and Jimenez, J.L. (2007) Elemental analysis of organic species with
 1219 electron ionization high-resolution mass spectrometry. *Anal. Chem.* 79, 8350-8358.
- 1220 Aiken, A.C., Decarlo, P.F., Kroll, J.H., Worsnop, D.R., Huffman, J.A., Docherty, K.S., Ulbrich,
 1221 I.M., Mohr, C., Kimmel, J.R., Sueper, D., Sun, Y., Zhang, Q., Trimborn, A., Northway,
 1222 M., Ziemann, P.J., Canagaratna, M.R., Onasch, T.B., Alfarra, M.R., Prevot, A.S.H.,
 1223 Dommen, J., Duplissy, J., Metzger, A., Baltensperger, U. and Jimenez, J.L. (2008) O/C
 1224 and OM/OC ratios of primary, secondary, and ambient organic aerosols with high-
 1225 resolution time-of-flight aerosol mass spectrometry. *Environ. Sci. Technol.* 42, 4478-
 1226 4485.
- 1227 Atkinson, R. and Arey, J. (2003) Atmospheric degradation of volatile organic compounds.
 1228 *Chem. Rev.* 103, 4605-4638.
- 1229 Bahreini, R., Middlebrook, A.M., de Gouw, J.A., Warneke, C., Trainer, M., Brock, C.A., Stark,
 1230 H., Brown, S.S., Dube, W.P., Gilman, J.B., Hall, K., Holloway, J.S., Kuster, W.C.,
 1231 Perring, A.E., Prevot, A.S.H., Schwarz, J.P., Spackman, J.R., Szidat, S., Wagner, N.L.,
 1232 Weber, R.J., Zotter, P. and Parrish, D.D. (2012) Gasoline emissions dominate over diesel
 1233 in formation of secondary organic aerosol mass. *Geophys. Res. Lett.* 39, L06805.
- 1234 Baker, K.R., Misenis, C., Obland, M.D., Ferrare, R.A., Scarino, A.J. and Kelly, J.T. (2013)
 1235 Evaluation of surface and upper air fine scale WRF meteorological modeling of the May
 1236 and June 2010 CalNex period in California. *Atmos. Environ.* 80, 299-309.
- 1237 Bertram, A.K., Martin, S.T., Hanna, S.J., Smith, M.L., Bodsworth, A., Chen, Q., Kuwata, M.,
 1238 Liu, A., You, Y. and Zorn, S.R. (2011) Predicting the relative humidities of liquid-liquid
 1239 phase separation, efflorescence, and deliquescence of mixed particles of ammonium
 1240 sulfate, organic material, and water using the organic-to-sulfate mass ratio of the particle
 1241 and the oxygen-to-carbon elemental ratio of the organic component. *Atmos. Chem. Phys.*
 1242 11, 10995-11006.
- 1243 Borbon, A., Gilman, J.B., Kuster, W.C., Grand, N., Chevaillier, S., Colomb, A., Dolgorouky, C.,
 1244 Gros, V., Lopez, M., Sarda-Estevé, R., Holloway, J., Stutz, J., Petetin, H., McKeen, S.,
 1245 Beekmann, M., Warneke, C., Parrish, D.D. and de Gouw, J.A. (2013) Emission ratios of
 1246 anthropogenic volatile organic compounds in northern mid-latitude megacities:
 1247 Observations versus emission inventories in Los Angeles and Paris. *J. Geophys. Res.-*
 1248 *Atmos.* 118, 2041-2057.
- 1249 Canagaratna, M.R., Jimenez, J.L., Kroll, J.H., Chen, Q., Kessler, S.H., Massoli, P., Hildebrandt
 1250 Ruiz, L., Fortner, E., Williams, L.R., Wilson, K.R., Surratt, J.D., Donahue, N.M., Jayne,
 1251 J.T. and Worsnop, D.R. (2015) Elemental ratio measurements of organic compounds
 1252 using aerosol mass spectrometry: characterization, improved calibration, and
 1253 implications. *Atmos. Chem. Phys.* 15, 253-272.
- 1254 Cappa, C.D. and Jimenez, J.L. (2010) Quantitative estimates of the volatility of ambient organic
 1255 aerosol. *Atmos. Chem. Phys.* 10, 5409-5424.

1256 Cappa, C.D., Onasch, T.B., Massoli, P., Worsnop, D.R., Bates, T.S., Cross, E.S., Davidovits, P.,
 1257 Hakala, J., Hayden, K.L., Jobson, B.T., Kolesar, K.R., Lack, D.A., Lerner, B.M., Li,
 1258 S.M., Mellon, D., Nuaaman, I., Olfert, J.S., Petaja, T., Quinn, P.K., Song, C.,
 1259 Subramanian, R., Williams, E.J. and Zaveri, R.A. (2012) Radiative Absorption
 1260 Enhancements Due to the Mixing State of Atmospheric Black Carbon. *Science* 337,
 1261 1078-1081.
 1262 Cappa, C.D. and Wilson, K.R. (2011) Evolution of organic aerosol mass spectra upon heating:
 1263 implications for OA phase and partitioning behavior. *Atmos. Chem. Phys.* 11, 1895-
 1264 1911.
 1265 Carlton, A.G. and Baker, K.R. (2011) Photochemical Modeling of the Ozark Isoprene Volcano:
 1266 MEGAN, BEIS, and Their Impacts on Air Quality Predictions. *Environ. Sci. Technol.* 45,
 1267 4438-4445.
 1268 Carlton, A.G., Bhave, P.V., Napelenok, S.L., Edney, E.D., Sarwar, G., Pinder, R.W., Pouliot,
 1269 G.A. and Houyoux, M. (2010) Model Representation of Secondary Organic Aerosol in
 1270 CMAQv4.7. *Environ. Sci. Technol.* 44, 8553-8560.
 1271 Carlton, A.G., Turpin, B.J., Altieri, K.E., Seitzinger, S.P., Mathur, R., Roselle, S.J. and Weber,
 1272 R.J. (2008) CMAQ model performance enhanced when in-cloud SOA is included:
 1273 comparisons of OC predictions with measurements. *Environ. Sci. Technol.* 42, 8798-
 1274 8802.
 1275 Carter, W.P.L. (2010) Development of the SAPRC-07 chemical mechanism. *Atmos. Environ.*
 1276 44, 5324-5335.
 1277 Chan, A.W.H., Kautzman, K.E., Chhabra, P.S., Surratt, J.D., Chan, M.N., Crouse, J.D., Kürten,
 1278 A., Wennberg, P.O., Flagan, R.C. and Seinfeld, J.H. (2009) Secondary organic aerosol
 1279 formation from photooxidation of naphthalene and alkylnaphthalenes: implications for
 1280 oxidation of intermediate volatility organic compounds (IVOCs). *Atmos. Chem. Phys.* 9,
 1281 3049-3060.
 1282 Chen, Q., Farmer, D.K., Schneider, J., Zorn, S.R., Heald, C.L., Karl, T.G., Guenther, A., Allan,
 1283 J.D., Robinson, N., Coe, H., Kimmel, J.R., Pauliquevis, T., Borrmann, S., Poschl, U.,
 1284 Andreae, M.O., Artaxo, P., Jimenez, J.L. and Martin, S.T. (2009) Mass spectral
 1285 characterization of submicron biogenic organic particles in the Amazon Basin. *Geophys.*
 1286 *Res. Lett.* 36, L20806.
 1287 Claeys, M., Szmigielski, R., Kourtchev, I., Van der Veken, P., Vermeylen, R., Maenhaut, W.,
 1288 Jaoui, M., Kleindienst, T.E., Lewandowski, M., Offenberg, J.H. and Edney, E.O. (2007)
 1289 Hydroxydicarboxylic Acids: Markers for Secondary Organic Aerosol from the
 1290 Photooxidation of α -Pinene. *Environ. Sci. Technol.* 41, 1628-1634.
 1291 de Gouw, J.A., Gilman, J.B., Borbon, A., Warneke, C., Kuster, W.C., Goldan, P.D., Holloway,
 1292 J.S., Peischl, J., Ryerson, T.B., Parrish, D.D., Gentner, D.R., Goldstein, A.H. and Harley,
 1293 R.A. (2012) Increasing atmospheric burden of ethanol in the United States. *Geophys.*
 1294 *Res. Lett.* 39, L15803.
 1295 de Gouw, J.A. and Jimenez, J.L. (2009) Organic Aerosols in the Earth's Atmosphere. *Environ.*
 1296 *Sci. Technol.* 43, 7614-7618.
 1297 DeCarlo, P.F., Ulbrich, I.M., Crouse, J., de Foy, B., Dunlea, E.J., Aiken, A.C., Knapp, D.,
 1298 Weinheimer, A.J., Campos, T., Wennberg, P.O. and Jimenez, J.L. (2010) Investigation of
 1299 the sources and processing of organic aerosol over the Central Mexican Plateau from
 1300 aircraft measurements during MILAGRO. *Atmos. Chem. Phys.* 10, 5257-5280.

1301 Docherty, K.S., Stone, E.A., Ulbrich, I.M., DeCarlo, P.F., Snyder, D.C., Schauer, J.J., Peltier,
1302 R.E., Weber, R.J., Murphy, S.M., Seinfeld, J.H., Grover, B.D., Eatough, D.J. and
1303 Jimenez, J.L. (2008) Apportionment of Primary and Secondary Organic Aerosols in
1304 Southern California during the 2005 Study of Organic Aerosols in Riverside (SOAR-1).
1305 Environ. Sci. Technol. 42, 7655-7662.

1306 Dockery, D.W. and Pope, C.A. (1994) Acute respiratory effects of particulate air-pollution.
1307 Annu. Rev. Publ. Health 15, 107-132.

1308 Donahue, N.M., Chuang, W., Epstein, S.A., Kroll, J.H., Worsnop, D.R., Robinson, A.L., Adams,
1309 P.J. and Pandis, S.N. (2013) Why do organic aerosols exist? Understanding aerosol
1310 lifetimes using the two-dimensional volatility basis set. Environmental Chemistry 10,
1311 151-157.

1312 Donahue, N.M., Robinson, A.L., Stanier, C.O. and Pandis, S.N. (2006) Coupled partitioning,
1313 dilution, and chemical aging of semivolatile organics. Environ. Sci. Technol. 40, 2635-
1314 2643.

1315 Dzepina, K., Cappa, C.D., Volkamer, R.M., Madronich, S., DeCarlo, P.F., Zaveri, R.A. and
1316 Jimenez, J.L. (2011) Modeling the Multiday Evolution and Aging of Secondary Organic
1317 Aerosol During MILAGRO 2006. Environ. Sci. Technol. 45, 3496-3503.

1318 Dzepina, K., Volkamer, R.M., Madronich, S., Tulet, P., Ulbrich, I.M., Zhang, Q., Cappa, C.D.,
1319 Ziemann, P.J. and Jimenez, J.L. (2009) Evaluation of recently-proposed secondary
1320 organic aerosol models for a case study in Mexico City. Atmos. Chem. Phys. 9, 5681-
1321 5709.

1322 Edney, E.O., Kleindienst, T.E., Jaoui, M., Lewandowski, M., Offenberg, J.H., Wang, W. and
1323 Claeys, M. (2005) Formation of 2-methyl tetrols and 2-methylglyceric acid in secondary
1324 organic aerosol from laboratory irradiated isoprene/NOX/SO2/air mixtures and their
1325 detection in ambient PM2.5 samples collected in the eastern United States. Atmos.
1326 Environ. 39, 5281-5289.

1327 El Haddad, I., Platt, S., Slowik, J.G., Mohr, C., Crippa, M., Temime-Roussel, B., Detournay, A.,
1328 Marchand, N., Baltensperger, U. and Prevot, A.S.H. (2012) *Contributions of Cooking*
1329 *Emissions to Primary and Secondary Organic Aerosol in Urban Atmospheres*, American
1330 Association for Aerosol Research 31st Annual Conference, Minneapolis, Minnesota
1331 <http://aarabstracts.com/2012/AbstractBook.pdf>

1332 Ensberg, J.J., Hayes, P.L., Jimenez, J.L., Gilman, J.B., Kuster, W.C., de Gouw, J.A., Holloway,
1333 J.S. and Seinfeld, J.H. (2014) Emission factor ratios, SOA mass yields, and the impact of
1334 vehicular emissions on SOA formation. Atmos. Chem. Phys. 14, 2383-2397.

1335 EPA (2013) *National Emissions Inventory*. Environmental Protection Agency
1336 <http://www.epa.gov/ttn/chief/net/2011inventory.html>

1337 Ervens, B. and Volkamer, R. (2010) Glyoxal processing by aerosol multiphase chemistry:
1338 towards a kinetic modeling framework of secondary organic aerosol formation in
1339 aqueous particles. Atmos. Chem. Phys. 10, 8219-8244.

1340 Fountoukis, C. and Nenes, A. (2007) ISORROPIA II: a computationally efficient
1341 thermodynamic equilibrium model for K⁺-Ca²⁺-Mg²⁺-NH₄⁺-Na⁺-SO₄²⁻-NO₃⁻-Cl⁻-
1342 H₂O aerosols. Atmos. Chem. Phys. 7, 4639-4659.

1343 Gentner, D.R., Isaacman, G., Worton, D.R., Chan, A.W.H., Dallmann, T.R., Davis, L., Liu, S.,
1344 Day, D.A., Russell, L.M., Wilson, K.R., Weber, R., Guha, A., Harley, R.A. and
1345 Goldstein, A.H. (2012) Elucidating secondary organic aerosol from diesel and gasoline

1346 vehicles through detailed characterization of organic carbon emissions. *Proc. Natl. Acad.*
1347 *Sci. U. S. A.* 109, 18318-18323.

1348 George, I.J. and Abbatt, J.P.D. (2010) Chemical evolution of secondary organic aerosol from
1349 OH-initiated heterogeneous oxidation. *Atmos. Chem. Phys.* 10, 5551-5563.

1350 Grieshop, A.P., Logue, J.M., Donahue, N.M. and Robinson, A.L. (2009) Laboratory
1351 investigation of photochemical oxidation of organic aerosol from wood fires 1:
1352 measurement and simulation of organic aerosol evolution. *Atmos. Chem. Phys.* 9, 1263-
1353 1277.

1354 Griffin, R.J., Chen, J.J., Carmody, K., Vutukuru, S. and Dabdub, D. (2007) Contribution of gas
1355 phase oxidation of volatile organic compounds to atmospheric carbon monoxide levels in
1356 two areas of the United States. *J. Geophys. Res.-Atmos.* 112, D10S17.

1357 Guzman-Morales, J., Frossard, A.A., Corrigan, A.L., Russell, L.M., Liu, S., Takahama, S.,
1358 Taylor, J.W., Allan, J., Coe, H., Zhao, Y. and Goldstein, A.H. (2014) Estimated
1359 contributions of primary and secondary organic aerosol from fossil fuel combustion
1360 during the CalNex and Cal-Mex campaigns. *Atmos. Environ.* 88, 330-340.

1361 Hallquist, M., Wenger, J.C., Baltensperger, U., Rudich, Y., Simpson, D., Claeys, M., Dommen,
1362 J., Donahue, N.M., George, C., Goldstein, A.H., Hamilton, J.F., Herrmann, H.,
1363 Hoffmann, T., Iinuma, Y., Jang, M., Jenkin, M.E., Jimenez, J.L., Kiendler-Scharr, A.,
1364 Maenhaut, W., McFiggans, G., Mentel, T.F., Monod, A., Prevot, A.S.H., Seinfeld, J.H.,
1365 Surratt, J.D., Szmigielski, R. and Wildt, J. (2009) The formation, properties and impact of
1366 secondary organic aerosol: current and emerging issues. *Atmos. Chem. Phys.* 9, 5155-
1367 5236.

1368 Hayes, P.L., Ortega, A.M., Cubison, M.J., Froyd, K.D., Zhao, Y., Cliff, S.S., Hu, W.W., Toohey,
1369 D.W., Flynn, J.H., Lefer, B.L., Grossberg, N., Alvarez, S., Rappenglück, B., Taylor,
1370 J.W., Allan, J.D., Holloway, J.S., Gilman, J.B., Kuster, W.C., de Gouw, J.A., Massoli, P.,
1371 Zhang, X., Liu, J., Weber, R.J., Corrigan, A.L., Russell, L.M., Isaacman, G., Worton,
1372 D.R., Kreisberg, N.M., Goldstein, A.H., Thalman, R., Waxman, E.M., Volkamer, R., Lin,
1373 Y.H., Surratt, J.D., Kleindienst, T.E., Offenberg, J.H., Dusanter, S., Griffith, S., Stevens,
1374 P.S., Brioude, J., Angevine, W.M. and Jimenez, J.L. (2013) Organic aerosol composition
1375 and sources in Pasadena, California during the 2010 CalNex campaign. *J. Geophys. Res.-*
1376 *Atmos.*, 9233-9257.

1377 Heald, C.L., Coe, H., Jimenez, J.L., Weber, R.J., Bahreini, R., Middlebrook, A.M., Russell,
1378 L.M., Jolleys, M., Fu, T.M., Allan, J.D., Bower, K.N., Capes, G., Crosier, J., Morgan,
1379 W.T., Robinson, N.H., Williams, P.I., Cubison, M.J., DeCarlo, P.F. and Dunlea, E.J.
1380 (2011) Exploring the vertical profile of atmospheric organic aerosol: comparing 17
1381 aircraft field campaigns with a global model. *Atmos. Chem. Phys.* 11, 12673-12696.

1382 Heald, C.L., Ridley, D.A., Kreidenweis, S.M. and Drury, E.E. (2010) Satellite observations cap
1383 the atmospheric organic aerosol budget. *Geophys. Res. Lett.* 37, L24808.

1384 Heo, J., de Foy, B., Olson, M.R., Pakbin, P., Sioutas, C. and Schauer, J.J. (2015) Impact of
1385 regional transport on the anthropogenic and biogenic secondary organic aerosols in the
1386 Los Angeles Basin. *Atmos. Environ.* 103, 171-179.

1387 Hersey, S.P., Craven, J.S., Schilling, K.A., Metcalf, A.R., Sorooshian, A., Chan, M.N., Flagan,
1388 R.C. and Seinfeld, J.H. (2011) The Pasadena Aerosol Characterization Observatory
1389 (PACO): chemical and physical analysis of the Western Los Angeles basin aerosol.
1390 *Atmos. Chem. Phys.* 11, 7417-7443.

1391 Hodzic, A. and Jimenez, J.L. (2011) Modeling anthropogenically-controlled secondary organic
1392 aerosols in a megacity: a simplified framework for global and climate models. *Geosci.*
1393 *Model Dev.* 4, 901-917.

1394 Hodzic, A., Jimenez, J.L., Madronich, S., Aiken, A.C., Bessagnet, B., Curci, G., Fast, J.,
1395 Lamarque, J.F., Onasch, T.B., Roux, G., Schauer, J.J., Stone, E.A. and Ulbrich, I.M.
1396 (2009) Modeling organic aerosols during MILAGRO: importance of biogenic secondary
1397 organic aerosols. *Atmos. Chem. Phys.* 9, 6949-6981.

1398 Hodzic, A., Jimenez, J.L., Madronich, S., Canagaratna, M.R., DeCarlo, P.F., Kleinman, L. and
1399 Fast, J. (2010a) Modeling organic aerosols in a megacity: potential contribution of semi-
1400 volatile and intermediate volatility primary organic compounds to secondary organic
1401 aerosol formation. *Atmos. Chem. Phys.* 10, 5491-5514.

1402 Hodzic, A., Jimenez, J.L., Prevot, A.S.H., Szidat, S., Fast, J.D. and Madronich, S. (2010b) Can
1403 3-D models explain the observed fractions of fossil and non-fossil carbon in and near
1404 Mexico City? *Atmos. Chem. Phys.* 10, 10997-11016.

1405 Hu, W.W., Hu, M., Yuan, B., Jimenez, J.L., Tang, Q., Peng, J.F., Hu, W., Shao, M., Wang, M.,
1406 Zeng, L.M., Wu, Y.S., Gong, Z.H., Huang, X.F. and He, L.Y. (2013) Insights on organic
1407 aerosol aging and the influence of coal combustion at a regional receptor site of central
1408 eastern China. *Atmos. Chem. Phys.* 13, 10095-10112.

1409 IPCC (2013) *Climate Change 2013: The Physical Scientific Basis*. Intergovernmental Panel on
1410 Climate Change: Working Group I, Geneva Switzerland

1411 Jaoui, M., Kleindienst, T.E., Lewandowski, M., Offenber, J.H. and Edney, E.O. (2005)
1412 Identification and Quantification of Aerosol Polar Oxygenated Compounds Bearing
1413 Carboxylic or Hydroxyl Groups. 2. Organic Tracer Compounds from Monoterpenes.
1414 *Environ. Sci. Technol.* 39, 5661-5673.

1415 Jathar, S.H., Gordon, T.D., Hennigan, C.J., Pye, H.O.T., Pouliot, G., Adams, P.J., Donahue,
1416 N.M. and Robinson, A.L. (2014) Unspeciated organic emissions from combustion
1417 sources and their influence on the secondary organic aerosol budget in the United States.
1418 *Proc. Natl. Acad. Sci. U. S. A.* 111, 10473-10478.

1419 Jathar, S.H., Miracolo, M.A., Tkacik, D.S., Donahue, N.M., Adams, P.J. and Robinson, A.L.
1420 (2013) Secondary Organic Aerosol Formation from Photo-Oxidation of Unburned Fuel:
1421 Experimental Results and Implications for Aerosol Formation from Combustion
1422 Emissions. *Environ. Sci. Technol.* 47, 12886-12893.

1423 Jimenez, J.L., Canagaratna, M.R., Donahue, N.M., Prevot, A.S.H., Zhang, Q., Kroll, J.H.,
1424 DeCarlo, P.F., Allan, J.D., Coe, H., Ng, N.L., Aiken, A.C., Docherty, K.S., Ulbrich, I.M.,
1425 Grieshop, A.P., Robinson, A.L., Duplissy, J., Smith, J.D., Wilson, K.R., Lanz, V.A.,
1426 Hueglin, C., Sun, Y.L., Tian, J., Laaksonen, A., Raatikainen, T., Rautiainen, J.,
1427 Vaattovaara, P., Ehn, M., Kulmala, M., Tomlinson, J.M., Collins, D.R., Cubison, M.J.,
1428 Dunlea, E.J., Huffman, J.A., Onasch, T.B., Alfarra, M.R., Williams, P.I., Bower, K.,
1429 Kondo, Y., Schneider, J., Drewnick, F., Borrmann, S., Weimer, S., Demerjian, K.,
1430 Salcedo, D., Cottrell, L., Griffin, R., Takami, A., Miyoshi, T., Hatakeyama, S., Shimono,
1431 A., Sun, J.Y., Zhang, Y.M., Dzepina, K., Kimmel, J.R., Sueper, D., Jayne, J.T., Herndon,
1432 S.C., Trimborn, A.M., Williams, L.R., Wood, E.C., Middlebrook, A.M., Kolb, C.E.,
1433 Baltensperger, U. and Worsnop, D.R. (2009) Evolution of Organic Aerosols in the
1434 Atmosphere. *Science* 326, 1525-1529.

1435 JRC (2011) *Emission Database for Global Atmospheric Research*. European Commission's Joint
1436 Research Centre <http://edgar.jrc.ec.europa.eu/overview.php?v=42>

1437 Kelly, J.T., Baker, K.R., Nowak, J.B., Murphy, J.G., Markovic, M.Z., VandenBoer, T.C., Ellis,
1438 R.A., Neuman, J.A., Weber, R.J. and Roberts, J.M. (2014) Fine-scale simulation of
1439 ammonium and nitrate over the South Coast Air Basin and San Joaquin Valley of
1440 California during CalNex-2010. *J. Geophys. Res.-Atmos.* 119, 3600-3614.

1441 Kleindienst, T.E., Jaoui, M., Lewandowski, M., Offenberg, J.H. and Docherty, K.S. (2012) The
1442 formation of SOA and chemical tracer compounds from the photooxidation of
1443 naphthalene and its methyl analogs in the presence and absence of nitrogen oxides.
1444 *Atmos. Chem. Phys.* 12, 8711-8726.

1445 Kleinman, L.I., Daum, P.H., Lee, Y.N., Senum, G.I., Springston, S.R., Wang, J., Berkowitz, C.,
1446 Hubbe, J., Zaveri, R.A., Brechtel, F.J., Jayne, J., Onasch, T.B. and Worsnop, D. (2007)
1447 Aircraft observations of aerosol composition and ageing in New England and Mid-
1448 Atlantic States during the summer 2002 New England Air Quality Study field campaign.
1449 *J. Geophys. Res.-Atmos.* 112, D09310.

1450 Knote, C., Hodzic, A. and Jimenez, J.L. (2014a) The effect of dry and wet deposition of
1451 condensable vapors on secondary organic aerosols concentrations over the continental
1452 US. *Atmos. Chem. Phys. Discuss.* 14, 13731-13767.

1453 Knote, C., Hodzic, A., Jimenez, J.L., Volkamer, R., Orlando, J.J., Baidar, S., Brioude, J., Fast, J.,
1454 Gentner, D.R., Goldstein, A.H., Hayes, P.L., Knighton, W.B., Oetjen, H., Setyan, A.,
1455 Stark, H., Thalman, R., Tyndall, G., Washenfelder, R., Waxman, E. and Zhang, Q.
1456 (2014b) Simulation of semi-explicit mechanisms of SOA formation from glyoxal in
1457 aerosol in a 3-D model. *Atmos. Chem. Phys.* 14, 6213-6239.

1458 Koo, B.Y., Ansari, A.S. and Pandis, S.N. (2003) Integrated approaches to modeling the organic
1459 and inorganic atmospheric aerosol components. *Atmos. Environ.* 37, 4757-4768.

1460 Kroll, J.H., Ng, N.L., Murphy, S.M., Flagan, R.C. and Seinfeld, J.H. (2006) Secondary organic
1461 aerosol formation from isoprene photooxidation. *Environ. Sci. Technol.* 40, 1869-1877.

1462 Lewis, C.W., Volckens, J., Braddock, J.N., Crews, W.S., Lonneman, W.A. and McNichol, A.P.
1463 (2006) Absence of ¹⁴C in PM_{2.5} Emissions from Gasohol Combustion in Small Engines.
1464 *Aerosol Sci. Technol.* 40, 657-663.

1465 Lim, H.J., Carlton, A.G. and Turpin, B.J. (2005) Isoprene forms secondary organic aerosol
1466 through cloud processing: Model simulations. *Environ. Sci. Technol.* 39, 4441-4446.

1467 Loza, C.L., Craven, J.S., Yee, L.D., Coggon, M.M., Schwantes, R.H., Shiraiwa, M., Zhang, X.,
1468 Schilling, K.A., Ng, N.L., Canagaratna, M.R., Ziemann, P.J., Flagan, R.C. and Seinfeld,
1469 J.H. (2014) Secondary organic aerosol yields of 12-carbon alkanes. *Atmos. Chem. Phys.*
1470 14, 1423-1439.

1471 Martin-Reviejo, M. and Wirtz, K. (2005) Is benzene a precursor for secondary organic aerosol?
1472 *Environ. Sci. Technol.* 39, 1045-1054.

1473 Matsunaga, A. and Ziemann, P.J. (2010) Gas-Wall Partitioning of Organic Compounds in a
1474 Teflon Film Chamber and Potential Effects on Reaction Product and Aerosol Yield
1475 Measurements. *Aerosol Sci. Technol.* 44, 881-892.

1476 McKeen, S., Chung, S.H., Wilczak, J., Grell, G., Djalalova, I., Peckham, S., Gong, W., Bouchet,
1477 V., Moffet, R., Tang, Y., Carmichael, G.R., Mathur, R. and Yu, S. (2007) Evaluation of
1478 several PM(2.5) forecast models using data collected during the ICARTT/NEAQS 2004
1479 field study. *J. Geophys. Res.-Atmos.* 112.

1480 Middlebrook, A.M., Bahreini, R., Jimenez, J.L. and Canagaratna, M.R. (2012) Evaluation of
1481 Composition-Dependent Collection Efficiencies for the Aerodyne Aerosol Mass
1482 Spectrometer using Field Data. *Aerosol Sci. Technol.* 46, 258-271.

1483 Mohr, C., DeCarlo, P.F., Heringa, M.F., Chirico, R., Slowik, J.G., Richter, R., Reche, C.,
1484 Alastuey, A., Querol, X., Seco, R., Peñuelas, J., Jiménez, J.L., Crippa, M., Zimmermann,
1485 R., Baltensperger, U. and Prévôt, A.S.H. (2011) Identification and quantification of
1486 organic aerosol from cooking and other sources in Barcelona using aerosol mass
1487 spectrometer data. *Atmos. Chem. Phys.* 11, 1649-1665.

1488 Murphy, B.N., Donahue, N.M., Fountoukis, C. and Pandis, S.N. (2011) Simulating the oxygen
1489 content of ambient organic aerosol with the 2D volatility basis set. *Atmos. Chem. Phys.*
1490 11, 7859-7873.

1491 Murphy, D.M., Cziczo, D.J., Froyd, K.D., Hudson, P.K., Matthew, B.M., Middlebrook, A.M.,
1492 Peltier, R.E., Sullivan, A., Thomson, D.S. and Weber, R.J. (2006) Single-particle mass
1493 spectrometry of tropospheric aerosol particles. *J. Geophys. Res.-Atmos.* 111, D23S32.

1494 Ng, N.L., Kroll, J.H., Chan, A.W.H., Chhabra, P.S., Flagan, R.C. and Seinfeld, J.H. (2007)
1495 Secondary organic aerosol formation from m-xylene, toluene, and benzene. *Atmos.*
1496 *Chem. Phys.* 7, 3909-3922.

1497 Ortega, A.M., Day, D.A., Cubison, M.J., Brune, W.H., Bon, D., de Gouw, J.A. and Jimenez, J.L.
1498 (2013) Secondary organic aerosol formation and primary organic aerosol oxidation from
1499 biomass-burning smoke in a flow reactor during FLAME-3. *Atmos. Chem. Phys.* 13,
1500 11551-11571.

1501 Parrish, D.D., Stohl, A., Forster, C., Atlas, E.L., Blake, D.R., Goldan, P.D., Kuster, W.C. and de
1502 Gouw, J.A. (2007) Effects of mixing on evolution of hydrocarbon ratios in the
1503 troposphere. *J. Geophys. Res.-Atmos.* 112, D10S34.

1504 Perraud, V., Bruns, E.A., Ezell, M.J., Johnson, S.N., Yu, Y., Alexander, M.L., Zelenyuk, A.,
1505 Imre, D., Chang, W.L., Dabdub, D., Pankow, J.F. and Finlayson-Pitts, B.J. (2012)
1506 Nonequilibrium atmospheric secondary organic aerosol formation and growth. *Proc. Natl.*
1507 *Acad. Sci. U. S. A.* 109, 2836-2841.

1508 Pye, H.O.T. and Seinfeld, J.H. (2010) A global perspective on aerosol from low-volatility
1509 organic compounds. *Atmos. Chem. Phys.* 10, 4377-4401.

1510 Renbaum-Wolff, L., Grayson, J.W., Bateman, A.P., Kuwata, M., Sellier, M., Murray, B.J.,
1511 Shilling, J.E., Martin, S.T. and Bertram, A.K. (2013) Viscosity of alpha-pinene secondary
1512 organic material and implications for particle growth and reactivity. *Proc. Natl. Acad.*
1513 *Sci. U. S. A.* 110, 8014-8019.

1514 Robinson, A.L., Donahue, N.M., Shrivastava, M.K., Weitkamp, E.A., Sage, A.M., Grieshop,
1515 A.P., Lane, T.E., Pierce, J.R. and Pandis, S.N. (2007) Rethinking organic aerosols:
1516 Semivolatile emissions and photochemical aging. *Science* 315, 1259-1262.

1517 Robinson, A.L., Subramanian, R., Donahue, N.M., Bernardo-Bricker, A. and Rogge, W.F.
1518 (2006) Source apportionment of molecular markers and organic aerosol. 3. Food cooking
1519 emissions. *Environ. Sci. Technol.* 40, 7820-7827.

1520 Ryerson, T.B., Andrews, A.E., Angevine, W.M., Bates, T.S., Brock, C.A., Cairns, B., Cohen,
1521 R.C., Cooper, O.R., de Gouw, J.A., Fehsenfeld, F.C., Ferrare, R.A., Fischer, M.L.,
1522 Flagan, R.C., Goldstein, A.H., Hair, J.W., Hardesty, R.M., Hostetler, C.A., Jimenez, J.L.,
1523 Langford, A.O., McCauley, E., McKeen, S.A., Molina, L.T., Nenes, A., Oltmans, S.J.,
1524 Parrish, D.D., Pederson, J.R., Pierce, R.B., Prather, K., Quinn, P.K., Seinfeld, J.H., Senff,
1525 C.J., Sorooshian, A., Stutz, J., Surratt, J.D., Trainer, M., Volkamer, R., Williams, E.J. and
1526 Wofsy, S.C. (2013) The 2010 California Research at the Nexus of Air Quality and
1527 Climate Change (CalNex) field study. *J. Geophys. Res.-Atmos.* 118, 5830-5866.

1528 Sarwar, G., Fahey, K., Kwok, R., Gilliam, R.C., Roselle, S.J., Mathur, R., Xue, J., Yu, J. and
1529 Carter, W.P.L. (2013) Potential impacts of two SO₂ oxidation pathways on regional
1530 sulfate concentrations: Aqueous-phase oxidation by NO₂ and gas-phase oxidation by
1531 Stabilized Criegee Intermediates. *Atmos. Environ.* 68, 186-197.

1532 Schauer, J.J., Kleeman, M.J., Cass, G.R. and Simoneit, B.R.T. (1999) Measurement of emissions
1533 from air pollution sources. 1. C-1 through C-29 organic compounds from meat
1534 charbroiling. *Environ. Sci. Technol.* 33, 1566-1577.

1535 Schauer, J.J., Kleeman, M.J., Cass, G.R. and Simoneit, B.R.T. (2002) Measurement of emissions
1536 from air pollution sources. 4. C-1-C-27 organic compounds from cooking with seed oils.
1537 *Environ. Sci. Technol.* 36, 567-575.

1538 Skamarock, W.C., Klemp, J.B., Dudhia, J., Gill, D.O., Barker, D.M., Duda, M.G., Huang, X.,
1539 Wang, W. and Powers, J.G. (2008) A description of the Advanced Reserch WRF version
1540 3. NCAR Technical Note NCAR/TN-475+STR.

1541 Slowik, J.G., Stroud, C., Bottenheim, J.W., Brickell, P.C., Chang, R.Y.W., Liggio, J., Makar,
1542 P.A., Martin, R.V., Moran, M.D., Shantz, N.C., Sjostedt, S.J., van Donkelaar, A.,
1543 Vlasenko, A., Wiebe, H.A., Xia, A.G., Zhang, J., Leaitch, W.R. and Abbatt, J.P.D. (2010)
1544 Characterization of a large biogenic secondary organic aerosol event from eastern
1545 Canadian forests. *Atmos. Chem. Phys.* 10, 2825-2845.

1546 Spracklen, D.V., Jimenez, J.L., Carslaw, K.S., Worsnop, D.R., Evans, M.J., Mann, G.W., Zhang,
1547 Q., Canagaratna, M.R., Allan, J., Coe, H., McFiggans, G., Rap, A. and Forster, P. (2011)
1548 Aerosol mass spectrometer constraint on the global secondary organic aerosol budget.
1549 *Atmos. Chem. Phys.* 11, 12109-12136.

1550 Sun, Y.L., Zhang, Q., Schwab, J.J., Demerjian, K.L., Chen, W.N., Bae, M.S., Hung, H.M.,
1551 Hogrefe, O., Frank, B., Rattigan, O.V. and Lin, Y.C. (2011) Characterization of the
1552 sources and processes of organic and inorganic aerosols in New York city with a high-
1553 resolution time-of-flight aerosol mass apectrometer. *Atmos. Chem. Phys.* 11, 1581-1602.

1554 Szmigielski, R., Surratt, J.D., Gómez-González, Y., Van der Veken, P., Kourtshev, I.,
1555 Vermeylen, R., Blockhuys, F., Jaoui, M., Kleindienst, T.E., Lewandowski, M.,
1556 Offenberg, J.H., Edney, E.O., Seinfeld, J.H., Maenhaut, W. and Claeys, M. (2007) 3-
1557 methyl-1,2,3-butanetricarboxylic acid: An atmospheric tracer for terpene secondary
1558 organic aerosol. *Geophys. Res. Lett.* 34, L24811.

1559 Tsimpidi, A.P., Karydis, V.A., Zavala, M., Lei, W., Molina, L., Ulbrich, I.M., Jimenez, J.L. and
1560 Pandis, S.N. (2010) Evaluation of the volatility basis-set approach for the simulation of
1561 organic aerosol formation in the Mexico City metropolitan area. *Atmos. Chem. Phys.* 10,
1562 525-546.

1563 Tunved, P., Hansson, H.C., Kerminen, V.M., Strom, J., Dal Maso, M., Lihavainen, H., Viisanen,
1564 Y., Aalto, P.P., Komppula, M. and Kulmala, M. (2006) High natural aerosol loading over
1565 boreal forests. *Science* 312, 261-263.

1566 Volkamer, R., Jimenez, J.L., Martini, F.S., Dzepina, K., Zhang, Q., Salcedo, D., Molina, L.T.,
1567 Worsnop, D.R. and Molina, M.J. (2006) Secondary Organic Aerosol Formation from
1568 Anthropogenic Air Pollution: Rapid and Higher than Expected. *Geophys. Res. Lett.* 33,
1569 L17811.

1570 Volkamer, R., San Martini, F., Molina, L.T., Salcedo, D., Jimenez, J.L. and Molina, M.J. (2007)
1571 A missing sink for gas-phase glyoxal in Mexico City: Formation of secondary organic
1572 aerosol. *Geophys. Res. Lett.* 34, L19807.

1573 Volkamer, R., Ziemann, P.J. and Molina, M.J. (2009) Secondary Organic Aerosol Formation
1574 from Acetylene (C₂H₂): seed effect on SOA yields due to organic photochemistry in
1575 the aerosol aqueous phase. *Atmos. Chem. Phys.* 9, 1907-1928.

1576 Wang, Q., Shao, M., Zhang, Y., Wei, Y., Hu, M. and Guo, S. (2009) Source apportionment of
1577 fine organic aerosols in Beijing. *Atmos. Chem. Phys.* 9, 8573-8585.

1578 Warneke, C., de Gouw, J.A., Holloway, J.S., Peischl, J., Ryerson, T.B., Atlas, E., Blake, D.,
1579 Trainer, M. and Parrish, D.D. (2012) Multiyear trends in volatile organic compounds in
1580 Los Angeles, California: Five decades of decreasing emissions. *J. Geophys. Res.-Atmos.*
1581 117, D00V17.

1582 Warneke, C., McKeen, S.A., de Gouw, J.A., Goldan, P.D., Kuster, W.C., Holloway, J.S.,
1583 Williams, E.J., Lerner, B.M., Parrish, D.D., Trainer, M., Fehsenfeld, F.C., Kato, S., Atlas,
1584 E.L., Baker, A. and Blake, D.R. (2007) Determination of urban volatile organic
1585 compound emission ratios and comparison with an emissions database. *J. Geophys. Res.-*
1586 *Atmos.* 112, D10S47.

1587 Washenfelder, R.A., Young, C.J., Brown, S.S., Angevine, W.M., Atlas, E.L., Blake, D.R., Bon,
1588 D.M., Cubison, M.J., de Gouw, J.A., Dusanter, S., Flynn, J., Gilman, J.B., Graus, M.,
1589 Griffith, S., Grossberg, N., Hayes, P.L., Jimenez, J.L., Kuster, W.C., Lefer, B.L., Pollack,
1590 I.B., Ryerson, T.B., Stark, H., Stevens, P.S. and Trainer, M.K. (2011) The glyoxal budget
1591 and its contribution to organic aerosol for Los Angeles, California, during CalNex 2010.
1592 *J. Geophys. Res.-Atmos.* 116, D00V02.

1593 Watson, J.G. (2002) Visibility: Science and regulation. *J. Air Waste Manage. Assoc.* 52, 628-
1594 713.

1595 Yarwood, G., Jung, J., Whitten, G.Z., Heo, G., Mellberg, J., Estes, E. (2010) *Updates to the*
1596 *Carbon Bond Mechanism for Version 6 (CB6). Presented at the 9th Annual CMAS*
1597 *Conference, Chapel, Hill, NC. ENVIRON International Corporation, Novato*
1598 http://www.camx.com/publ/pdfs/CB05_Final_Report_120805.pdf

1599 Yatavelli, R.L.N., Stark, H., Thompson, S.L., Kimmel, J.R., Cubison, M.J., Day, D.A.,
1600 Campuzano-Jost, P., Palm, B.B., Hodzic, A., Thornton, J.A., Jayne, J.T., Worsnop, D.R.
1601 and Jimenez, J.L. (2014) Semicontinuous measurements of gas-particle partitioning of
1602 organic acids in a ponderosa pine forest using a MOVI-HRToF-CIMS. *Atmos. Chem.*
1603 *Phys.* 14, 1527-1546.

1604 Zhang, Q., Jimenez, J.L., Canagaratna, M.R., Allan, J.D., Coe, H., Ulbrich, I., Alfarra, M.R.,
1605 Takami, A., Middlebrook, A.M., Sun, Y.L., Dzepina, K., Dunlea, E., Docherty, K.,
1606 DeCarlo, P.F., Salcedo, D., Onasch, T., Jayne, J.T., Miyoshi, T., Shimojo, A.,
1607 Hatakeyama, S., Takegawa, N., Kondo, Y., Schneider, J., Drewnick, F., Borrmann, S.,
1608 Weimer, S., Demerjian, K., Williams, P., Bower, K., Bahreini, R., Cottrell, L., Griffin,
1609 R.J., Rautiainen, J., Sun, J.Y., Zhang, Y.M. and Worsnop, D.R. (2007) Ubiquity and
1610 dominance of oxygenated species in organic aerosols in anthropogenically-influenced
1611 Northern Hemisphere midlatitudes. *Geophys. Res. Lett.* 34, L13801.

1612 Zhang, X., Cappa, C.D., Jathar, S.H., McVay, R.C., Ensberg, J.J., Kleeman, M.J. and Seinfeld,
1613 J.H. (2014) Influence of vapor wall loss in laboratory chambers on yields of secondary
1614 organic aerosol. *Proc. Natl. Acad. Sci. U. S. A.* 111, 5802-5807.

1615 Zhang, X., Liu, J., Parker, E.T., Hayes, P.L., Jimenez, J.L., de Gouw, J.A., Flynn, J.H.,
1616 Grossberg, N., Lefer, B.L. and Weber, R.J. (2012) On the gas-particle partitioning of
1617 soluble organic aerosol in two urban atmospheres with contrasting emissions: 1. Bulk
1618 water-soluble organic carbon. *J. Geophys. Res.-Atmos.* 117, D00V16.

1619 Zhao, Y., Hennigan, C.J., May, A.A., Tkacik, D.S., de Gouw, J.A., Gilman, J.B., Kuster, W.C.,
1620 Borbon, A. and Robinson, A.L. (2014) Intermediate-Volatility Organic Compounds: A
1621 Large Source of Secondary Organic Aerosol. *Environ. Sci. Technol.* 48, 13743-13750.
1622 Zotter, P., El-Haddad, I., Zhang, Y., Hayes, P.L., Zhang, X., Lin, Y.-H., Wacker, L., Schnelle-
1623 Kreis, J., Abbaszade, G., Zimmermann, R., Surratt, J.D., Weber, R., Jimenez, J.L., Szidat,
1624 S., Baltensperger, U. and Prévôt, A.S.H. (2014) Diurnal cycle of fossil and nonfossil
1625 carbon using radiocarbon analyses during CalNex. *J. Geophys. Res.-Atmos.* 119, 6818-
1626 6835.

1627

1628

1629 **Table 1.** Definitions of acronyms frequently used in this article.

AMS	Aerosol Mass Spectrometer
BG-SOA	Background secondary organic aerosols
CalNex	California research at the nexus of air quality and climate change field campaign
CIOA	Cooking-influenced organic aerosol
GRI	Grieshop et al. (2009) parameterization for secondary organic aerosol formation from P-S/IVOCs
IVOCs	Intermediate volatility organic compounds
NEI	National Emissions Inventory
OA	Organic aerosol
ODR	Orthogonal distance regression
PAH	Polycyclic aromatic hydrocarbon
PBL	Planetary Boundary Layer
P-S/IVOCs	Primary semi-volatile and intermediate volatility organic compounds
PYE	Pye and Seinfeld (2010) parameterization for secondary organic aerosols formation from P-S/IVOCs
ROB	Robinson et al. (2007) parameterization for secondary organic aerosol formation from P-S/IVOCs
SI-SOA	Secondary organic aerosol from primary semi-volatile and intermediate volatility organic compounds
SOA	Secondary organic aerosol
SVOCs	Semi-volatile organic compounds
TSI	Tsimpidi et al. (2010) parameterization for secondary organic aerosol formation from VOCs
V-SOA	Secondary organic aerosol formed from the oxidation of volatile organic compounds
VBS	Volatility basis set
VOCs	Volatile organic compounds
WRF-CMAQ	Weather Research Forecasting – Community multiscale air quality model
Δ CO	Enhanced CO concentration over the background concentration (105 ppb).

1631 **Table 2.** Summary of the SOA models and their major variants used in this work.

Model Name	Variation	Notes	References	Figures
Box Model	1 (ROB + TSI)	VOCs: Tsimpidi et al. parameterization <u>with aging</u> . P-S/IVOCs: Robinson et al. parameterization, and all SOA treated within VBS framework.	Tsimpidi et al. <i>Atmos. Chem. Phys.</i> 2010 , 525-546. Robinson et al. <i>Science</i> 2007 , 1259-1262.	4, 6, 7, 8, 10, SI-2, SI-5, SI-6, SI-7
	2 (GRI + TSI)	VOCs: Tsimpidi et al. parameterization <u>with aging</u> . P-S/IVOCs: Grieshop et al. parameterization, and all SOA treated within VBS framework.	Tsimpidi et al. <i>Atmos. Chem. Phys.</i> 2010 , 525-546. Grieshop et al. <i>Science</i> 2009 , 1263-1277.	4, 5, 6, 7, 8, 10, SI-2, SI-5, SI-6, SI-7
	3 (PYE + TSI)	VOCs: Tsimpidi et al. parameterization <u>with aging</u> . P-S/IVOCs: Pye and Seinfeld parameterization.	Tsimpidi et al. <i>Atmos. Chem. Phys.</i> 2010 , 525-546. Pye and Seinfeld <i>Atmos. Chem. Phys.</i> 2010 , 4377-4401.	4, 6, 7, 8, SI-2, SI-5, SI-6, SI-7
	4 (ROB + 4xV)	VOCs: Tsimpidi et al. parameterization <u>without aging</u> and aromatic yield multiplied by 4. P-S/IVOCs: Robinson et al. parameterization, and all SOA treated within VBS framework.	Tsimpidi et al. <i>Atmos. Chem. Phys.</i> 2010 , 525-546. Robinson et al. <i>Science</i> 2007 , 1259-1262. Zhang et al. <i>PNAS</i> 2014 .	4, 6, 7, 8, SI-5, SI-6, SI-7
	5	VOCs: Koo et al. and Ng et al. wherein SOA is treated in a lumped product parameterization.	Koo et al. <i>Atmos. Environ.</i> 2003 , 4757-4768. Ng et al. <i>Atmos. Chem. Phys.</i> 2007 , 3909-3922.	8

1632

1633 **Table 2 (Continued).** Summary of the SOA models and their major variants used in this work.

Model Name	Variation	Notes	References	Figures
WRF-CMAQ	v5.0.1	4 anthropogenic VOC and 3 biogenic VOC precursors and GLY/MGLY. 12 semi-volatile partitioning species and 7 non-volatile SOA species	Carlton et al. <i>Environ. Sci. Technol.</i> 2010 , 8553-8560.	9, SI-8, SI-9, SI-10
SIMPLE	N/A	Single lumped precursor and single lumped, non-volatile SOA product.	Hodzic et al. <i>Geosci. Model Dev.</i> 2011 , 901-917.	7, 8, 11, 12
WRF-Chem	N/A	4-bin VBS framework <u>with aging</u> , 7 anthropogenic VOC classes and 4 biogenic VOC classes	Ahmadov et al. <i>J. Geophys. Res.-Atmos.</i> 2012 , D06301.	3, SI-4

1634

1635 **Table 3.** Measurements acquired at the Pasadena ground site during CalNex and used in this
 1636 study.

Measurement	Technique	Uncertainty	Reference
Bulk aerosol mass concentrations for organics, nitrate, sulfate, and ammonium as well as the concentrations of organic aerosol components	High-resolution Aerosol Mass Spectrometry (AMS) and Positive Matrix Factorization (PMF) analysis	±30%	Hayes et al. 2013
Oxygen-to-carbon ratio	High-resolution Aerosol Mass Spectrometer (AMS) and Elemental Analysis (EA)	±30%	Hayes et al. 2013
Speciated VOCs	Gas chromatography – mass spectrometry	±5 – 25% (hydrocarbons) ±20 – 35% (oxygenates)	Borbon et al. 2013
CO	VUV Fluorescence	±4%	Hayes et al. 2013
Modern and fossil fraction of organic carbon	¹⁴ C	See text	Zotter et al. 2014
Concentration of SOA from specific precursor compounds	U.S. E.P.A. tracer method and measurement of oxygenates from filter samples using GC-MS	See text	Kleindienst et al. 2012
Concentration of naphthalene and its derivatives	Thermal desorption gas chromatography mass spectrometry	±30%	Presto et al. 2011 Presto et al. 2012

1637

1638 **Table 4.** Slope of SOA/ Δ CO as reported by Hayes et al. (2013), and as predicted in the four
 1639 major box model variations. For the box model, the slopes are obtained by performing a linear
 1640 ODR analysis on the data shown in Figure 7.

Variation	SOA / Δ CO slope between 0 and 0.25 Days	SOA / Δ CO slope between 0.25 and 0.5 Days
Observed (Hayes et al. 2013)	$108 \mu\text{g m}^{-3}$	
ROB + TSI	$69 \mu\text{g m}^{-3} \text{ppmv}^{-1}$	$88 \mu\text{g m}^{-3} \text{ppmv}^{-1}$
GRI + TSI	$110 \mu\text{g m}^{-3} \text{ppmv}^{-1}$	$130 \mu\text{g m}^{-3} \text{ppmv}^{-1}$
PYE + TSI	$168 \mu\text{g m}^{-3} \text{ppmv}^{-1}$	$153 \mu\text{g m}^{-3} \text{ppmv}^{-1}$
ROB + 4xV	$105 \mu\text{g m}^{-3} \text{ppmv}^{-1}$	$123 \mu\text{g m}^{-3} \text{ppmv}^{-1}$

1641

1642 **Figure Captions**

1643 **Figure 1.** Schematic of the major SOA parameterizations used in the box model. The different
1644 regions of the volatility scale are indicated on the top axis: low-volatility organic compounds
1645 (LVOCs), semi-volatile organic compounds (SVOCs), intermediate volatility organic
1646 compounds (IVOCs), and volatile organic compounds (VOCs). The fraction in the particle
1647 phase, F_p (top panel), increases with decreasing volatility (i.e. C^*) according to Equation 1. The
1648 campaign average OA concentration, $7 \mu\text{g m}^{-3}$, has been used to calculate the partitioning. The
1649 parameterization of Tsimpidi et al. (2010) distributes the VOC oxidation products into four
1650 volatility bins, and subsequent oxidation reactions are allowed as indicated by the curved arrows.
1651 The two parameterizations for P-S/IVOC oxidation from Robinson et al. (2007) and Grieshop et
1652 al. (2009) are illustrated as well. Lastly, the parameterization of Pye and Seinfeld (2010) is
1653 shown in which SVOCs are treated as four lumped species (pink), and IVOCs are treated using
1654 the yields and volatility distribution for naphthalene oxidation (yellow). For clarity the arrows
1655 indicating IVOC aging are not shown.

1656 **Figure 2.** Schematic of the SOA model set-up used in this work. Model inputs are indicated by
1657 hollow arrows whereas steps in the modeling process are indicated by solid arrow. All the steps
1658 in the dashed box are repeated for each hour of the day.

1659 **Figure 3. (A)** Average diurnal cycle of CO (red) and photochemical age (blue) for the Pasadena
1660 ground site during CalNex. Note: A background of 105 ppbv has been subtracted from the CO
1661 concentration. **(B)** Average diurnal cycle of the five OA components identified by PMF analysis,
1662 as well as the background OA calculated from WRF-Chem. The five components are semi-
1663 volatile oxygenated organic aerosol (SV-OOA), cooking-influenced organic aerosol (CIOA),
1664 hydrocarbon-like organic aerosol (HOA), local organic aerosol (LOA), and low volatility organic
1665 aerosol (LV-OOA).

1666 **Figure 4.** Model/measurement comparisons for urban SOA mass concentration plotted by time
1667 of day. The model results are shown for the **(ROB+TSI)**, **(GRI+TSI)**, **(PYE+TSI)**, and
1668 **(ROB+4xV)** variations. The model variations are described in Table 2. In all panels the SV-
1669 OOA determined from measurements at the Pasadena ground site is shown. The uncertainty for
1670 the AMS measurement used to determine the SV-OOA concentration is indicated by the dashed
1671 lines (Middlebrook et al., 2012).

1672 **Figure 5. (A)** Predicted SOA mass from precursor VOCs. For clarity only the five largest
1673 contributors to the SOA mass are shown. Note that SI-SOA from P-S/IVOCs is not included in
1674 this panel. **(B)** Campaign average concentrations of SOA from specific precursors as determined
1675 in the box model as well as by the U.S. EPA tracer method (Kleindienst et al., 2012).
1676 Comparisons are shown for methylbenzenes, naphthalenes, isoprene, and monoterpenes. For the
1677 naphthalenes the bar for “adjusted emissions” indicates the model variation where the
1678 naphthalene emissions are increased in order to match the measured concentrations in Pasadena
1679 as shown in Figure SI-3. The adjusted emissions are also used for the variation with a yield of
1680 1.5 at $C^*=1$. Note: The GRI parameterization is used to predict the SI-SOA for these results.

1681 **Figure 6.** The estimated fractional contribution to SOA mass concentration from gasoline
1682 vehicles, diesel vehicles, cooking emissions, and in-basin biogenic emissions. The results for the
1683 four model variations are displayed as pie charts as well as a bar chart. The bar chart also shows
1684 the percentage of SOA that is from fossil or modern sources as determined by Zotter et al.
1685 (2014). The modern sources are indicated by hollow bars and fossil sources are indicated by
1686 solid bars. Background SOA is not included in this figure, but the analogous figure with
1687 background SOA is given in Figure SI-6 of the supporting information.

1688 **Figure 7.** SOA concentration predicted by the ROB+TSI, GRI+TSI, PYE+TSI, and ROB+4xV
1689 parameterizations for up to 3 days of photochemical aging at a reference $\bullet\text{OH}$ concentration of
1690 $1.5 \times 10^6 \text{ molec cm}^{-3}$. Also shown in the four panels is the same result for the SIMPLE model
1691 using the optimized parameters. Note that the SOA concentrations have been normalized to the
1692 background subtracted CO concentration to account for changes in emission strengths, and the
1693 processed data are identified by the symbol $\text{SOA}/\Delta\text{CO}$. In addition, the $\text{SOA}/\Delta\text{CO}$ data
1694 determined for the Pasadena site from the measurements of Hayes et al. (2013) are shown as well
1695 as similar airborne measurements for the Los Angeles basin outflow performed by Bahreini et al.
1696 (2012) aboard the NOAA P3 (black marker). The Bahreini et al. data point corresponds to an
1697 average of all data between 1 – 2 days of photochemical aging. The $\text{OA}/\Delta\text{CO}$ ratio reported by
1698 de Gouw and Jimenez (2009) is also indicated (gray box) to serve as an estimate of $\text{SOA}/\Delta\text{CO}$
1699 in highly aged air masses. ~~For clarity, the uncertainty in the SOA determined from measurements~~
1700 ~~($\pm 30\%$) is not shown.~~

1701

1702 **Figure 8.** SOA concentration predicted by the ROB+TSI, GRI+TSI, PYE+TSI, and ROB+4xV
1703 parameterizations for up to 3 days of photochemical aging at a reference •OH concentration of
1704 1.5×10^6 molec cm⁻³. These predictions correspond to the sensitivity study in which the
1705 concentration of IVOCs in the volatility bins $C^* = 10^3 - 10^6$ were reduced by one-half. Also
1706 shown in the three panels is the same result for the SIMPLE model using the optimized
1707 parameters (see Section 3.3 for further discussion). Note that the SOA concentrations have been
1708 normalized to the background subtracted CO concentration to account for changes in emission
1709 strengths, and the processed data are identified by the symbol SOA/ Δ CO. In addition, the
1710 SOA/ Δ CO data determined for the Pasadena site from the measurements of Hayes et al. (2013)
1711 are shown (black line) as well as similar airborne measurements downwind of Pasadena
1712 performed by Bahreini et al. (2012) aboard the NOAA P3 (black marker). The Bahreini et al.
1713 point corresponds to an average of all LA Basin outflow data between 1 – 2 days of
1714 photochemical aging. The OA/ Δ CO ratio reported by de Gouw and Jimenez (2009) is also
1715 indicated (gray box) to serve as an estimate of SOA/ Δ CO in highly aged air masses.

1716 **Figure 98.** (A) Scatter plot of SOA predicted by the WRF-CMAQ model versus the OOA
1717 determined from measurements at the Pasadena ground site. Also shown in this panel is an ODR
1718 linear regression analysis of the data with the y-intercept fixed to zero. (B) SOA diurnal cycles
1719 from the WRF-CMAQ and box model. The box model was run using an empirical two product
1720 parameterization (i.e., Model Variant 5 in Table 2) wherein the oxidized products cannot
1721 undergo aging (Dzepina et al., 2009).

1722 **Figure 109.** Model/measurement comparison for O:C of total OA versus time of day. The left
1723 panel contains the results when using the ROB+TSI model variation, whereas the right panel
1724 contains the results when using the GRI+TSI model variation. In both panels the O:C of OA
1725 measured at the Pasadena ground site is shown along with the O:C uncertainty. Shown in both
1726 panels is the model O:C when including only the SOA from VOCs (blue line), and the model
1727 O:C when including the SOA from both VOCs and P-S/IVOCs (pink line).

1728 **Figure 110.** (A) Image plot of the root mean square error between the SIMPLE urban SOA
1729 parameterization concentration and the measured SV-OOA as a function of both the lumped
1730 precursor emission ratio and the oxidation rate constant. The gray stars indicate the parameter
1731 pairs that result in the minimum errors for Pasadena (this study) and Mexico City (Hodzic and

1732 Jimenez, 2011). The dashed box approximately indicates the range of possible optimal parameter
1733 combinations. For reference an emission ratio of $80 \mu\text{g m}^{-3} \text{ppmv}^{-1}$ equals 0.069 g g^{-1} . (B)
1734 Diurnal cycle of SV-OOA with corresponding uncertainty (grey dashed lines). The diurnal cycle
1735 of SOA predicted by the SIMPLE model is shown as well.

1736 | **Figure 121.** Model/measurement comparison of O:C of OA versus time of day for the SIMPLE
1737 urban SOA parameterization. The original parameterization proposed by Hodzic and Jimenez
1738 (2011) is $\text{O:C} = 1 - 0.6\exp(-A/1.5)$, where A is the photochemical age. The updated SIMPLE
1739 parameterization is $\text{O:C} = 1.28(1 - 0.6\exp(-A/1.5))$, which accounts for the updated AMS O:C
1740 calibration factors.